The Use of Nanobead Technology to Deliver Zoledronic Acid to Prostate Cancer Cell Lines

Bardia Barimani, BSc (Hons) MBBS

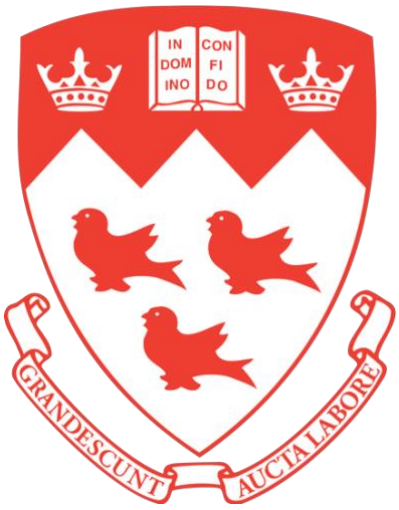

Division of Orthopedic Surgery

Department of Surgery

Division of Experimental Surgery, McGill University, Montreal, QC, Canada

November 2019

A thesis submitted to the Faculty of Graduate Studies and Research at McGill University in partial fulfillment of the requirements of the degree of Master of Science in Experimental Surgery

Abstract

Background Up to 80% of patients with primary tumors of the breast, prostate or lung will develop spine metastases. Spine metastases cause pain, functional deficit and severely diminished health related quality of life through fracture, vertebral instability and spinal cord and nerve-root compression. This is associated with high socioeconomic and healthcare costs. With advancements in medical, radiation and surgical oncology, these patients are living longer thereby increasing the disease burden. Surgical bone resection of metastatic tumors leads to large bone defects that cannot self-repair, and treatment with antiresorptive bisphosphonates such as Zoledronate, is being explored for tissue repair. However, bone loss, instability and poor repair following tumor resection remains an unmet clinical need in this population. This leads to the possibility of exploring nanotechnology to delivery drugs locally and at therapeutic to help with the management of spine tumor patients.

Methods We first investigated the proliferation of various prostate cancer cell lines; LAPC4, 22RV1 and PC3 with different doses of Zoledronate using Alamarblue® kit and MTT assays. Following this we performed migration assays on similar cell lines using Boyden chambers and scratch assays.

Once the action of various Zoledronate doses were established we worked to coat silica nanobeads with this drug and assess its release. The silica nanobeads were first prepared and tested using fluorescently labelled Zoledronate. Once a reproducible protocol was established, we tested the release of nanobeads coated in Zoledronate in a 3D bioprinted in-vitro model using a prostate cancer

cell line (C42B). The coated nanobeads were placed in the middle of the 3D construct surrounded by the prostate cancer cell. The proliferation of these cells was then assessed to determine the local release and activity of Zoledronate coated nanobeads.

Results The highest dose of Zoledronate (100 µM) was found to reduce the proliferation of the prostate cancer cell lines LAPC4 and PC3 over 48 hours (0.711 ± 0.180 p value = 0.0497 and 0.575 ± 0.212, p=0.02571 respectively). No significant effect was found on the 22RV1 cell line over 48 hours with all Zoledronate concentrations tested. Proliferation of osteoblast cells were also reduced at Zoledronate 100 µM concentration (0.698 ± 0.0.52, p value = 0.0145). Cell migration was reduced with 10 µM for LAPC4 cells using the Boyden chamber (22.8% ± 8.1, p value = 0.04) and with 100 µM for PC3 cells performed using scratch assay over 24 and 48 hours (ratio 0.443 ± 0.024, p value = 0.047 and 0.375 ± 0.003, p value = 0.002 respectively).

The nanobeads were tested firstly using fluorescently labelled Zoledronate and it was found that chitosan coated nanobeads retain and deliver more of the drug per day for a total of 8 days (302.1 µM cumulatively). Following this, we found that Zoledronate coated nanobeads placed in a 3D bioprinted construct with C42B prostate cancer cell lines shows a reducing trend in the proliferation of that cell line over 7 days.

Conclusion Our experiments showed extremely promising results in using nanobeads as an inexpensive drug delivery system, both locally and at therapeutic levels. We elaborated on the action of Zoledronate on the activity of various prostate cancer cell lines. In addition to this, we devised a

successful protocol enabling us to coat silica nanobeads with Zoledronate and show its local delivery and therapeutic action in a 3D bioprinted construct with a prostate cancer cell line. We feel this will be the steppingstone for our future vision in relation to the local delivery of bisphosphonates to tumor cells. We foresee the future to involve spinal metastasis mice models and the integration of these coated nanobeads in a structurally stable construct such as bone cement to fill the void following spine tumor resection.

Résumé

Contexte Jusqu'à 80% des patients atteints de tumeurs primitives du sein, de la prostate ou du poumon développeront des métastases de la colonne vertébrale. Les métastases de la colonne vertébrale provoquent de la douleur, un déficit fonctionnel et une qualité de vie liée à la santé fortement dégradée par le biais de fractures, une instabilité vertébrale et une compression de la colonne vertébrale et des racines nerveuses. Ceci est associé à des coûts socio-économiques et de santé élevés. Avec les progrès réalisés en oncologie médicale, radiologique et chirurgicale, ces patients vivent plus longtemps, augmentant ainsi le fardeau de la maladie. La résection osseuse chirurgicale des tumeurs métastatiques conduit à des défauts osseux importants qui ne peuvent pas s'auto-réparer, et un traitement par des bisphosphonates antirésorptifs, tels que le zolédronate, est actuellement à l'étude pour la réparation des tissus. Cependant, la perte osseuse, l'instabilité et la mauvaise réparation après la résection de la tumeur restent un besoin clinique non satisfait dans cette population. Cela conduit à la possibilité d'utiliser des nanotechnologies pour administrer des médicaments localement et de manière thérapeutique afin de faciliter la gestion des patients atteints de tumeur à la colonne vertébrale.

Méthodes Nous avons initialement effectué des expériences montrant la prolifération de différentes lignées cellulaires du cancer de la prostate; LAPC4, 22RV1 et PC3 avec différentes doses de zolédronate en utilisant le kit Alamarblue® et les tests MTT. Après cela, nous avons effectué des tests de migration sur des lignées cellulaires similaires en utilisant des chambres de Boyden et des tests de grattage.

Une fois que l'action de diverses doses de zolédronate a été établie, nous avons travaillé pour recouvrir ce médicament de nanobilles de silice et évaluer sa libération. Les nanobilles de silice ont d'abord été préparées et testées à l'aide de zolédronate marqué par une fluorescence. Une fois que le protocole établi a été mis au point, nous avons commencé à tester la libération de nanobilles enrobées de zolédronate dans un modèle in vitro bioimprimé en 3D fabriqué à partir d'une lignée cellulaire du cancer de la prostate. Les nanobilles enrobées ont été placées au milieu de la construction 3D entourée par la cellule cancéreuse de la prostate. La prolifération de ces cellules a ensuite été évaluée pour comprendre la libération et l'activité locales des nanobilles enrobées de zolédronate.

Résultats La dose la plus élevée de zolédronate (100 µM) s'est avérée réduire la prolifération des cellules cancéreuses de la prostate LAPC4 et PC3 en 48 heures (0,711 ± 0,180 valeur p = 0,0497 et 0,575 ± 0,212, p = 0,02571 respectivement). Aucun effet significatif n'a été observé sur la lignée cellulaire 22RV1 sur une période de 48 heures avec toutes les concentrations de zolédronate testées. La prolifération des cellules d'ostéoblastes a également été réduite à une concentration de Zolédronate de 100 µM (0,698 ± 0,0,52, valeur p = 0,0145). La migration cellulaire a été réduite avec 10 µM pour les cellules LAPC4 à l'aide de la chambre de Boyden (22,8% ± 8,1, valeur p = 0,04) et avec 100 µM pour les cellules PC3 réalisées par test de scratch sur 24 et 48 heures (rapport 0,443 ± 0,024, valeur p 0,047 et 0,375 ± 0,003, p = 0,002 respectivement).

Les nanobilles ont tout d'abord été testées avec du zolédronate marqué par une fluorescence et il a été constaté que les nanobilles enrobées de chitosane retiennent et délivrent un total de 8 jours

(302,1 µM de façon cumulée). Suite à cela, nous avons constaté que les nanobilles enrobées de zolédronate placées dans une construction 3D imprimée avec une lignée cellulaire de cancer de la prostate C42B réduisaient la prolifération de cette lignée cellulaire en 7 jours.

Conclusion Nos expériences ont montré des résultats extrêmement précieux en ce qui concerne la possibilité d'utiliser la nanotechnologie comme vecteur pour administrer un médicament à moindre coût, localement et à des niveaux thérapeutiques. Nous avons détaillé l'activité du zolédronate sur l'activité de diverses lignées cellulaires du cancer de la prostate. En outre, nous avons mis au point un protocole efficace nous permettant de revêtir Zoledroante de nanophares de silice et d'en montrer la distribution locale dans une construction bioprintée 3D avec une lignée de cellules cancéreuses de la prostate. Nous pensons que ce sera le tremplin de notre vision future en ce qui concerne l'administration libre de bisphosphonates dans les cellules tumorales. Nous prévoyons que l'avenir impliquera des modèles de souris atteintes de métastases vertébrales et l'intégration de ces nanobilles enrobées dans une construction structurellement stable telle que le ciment osseux pour combler le vide après la résection tumorale de la colonne vertébrale.

Table of Contents

Acknowledgements

I would like to express a special thank you to my supervisor Dr Michael Weber for his continuous support and backing. He has always been available and of great support throughout my Master's and will continue to be a valuable mentor throughout my career.

I would also like to thank my co-supervisor Dr Lisbet Haglund and Dr Derek Rosenzweig for their support throughout this passage and their huge impact on my work.

I thank my fellow colleagues and lab mates who have been of upmost help and support throughout my project. A special thank you goes to Dr Pouyan Ahangar, a great colleague and friend, for his kind support throughout this journey. A thank you also goes to Dr Elie Akoury, Dr Janet Moir and Dr Megan Cooke for for their great teaching and troubleshooting, setting me in a position to perform my experiments.

Finally, I would like to thank my family and friends for their continuous support and encouragement throughout my years of studying and pursuit of my goals.

Contributions of Authors

This work consists of 1 manuscript in preparation for publication by the supervisor and candidate.

Bardia Barimani (candidate): performed the experimental work consisting of Zoledronate activity on cancer cell, formation of drug coated nanobeads, 3D bioprinted constructs, data collection, literature review, data analysis, writing the manuscript

Dr Michael Weber (primary investigator): he was the main supervisor throughout the Master's and was responsible for the candidate and thesis completion throughout this process. He provided insightful ideas, guidance, lab space and supervision.

Dr Lisbet Haglund (co-supervisor): provided detailed knowledge and ideas throughout my study. She devised ideas which were critical to the success of this study.

Contributions of statements of Originality

The work described here was performed by the author and is original. This manuscript is the first report that describes the use of nanobead technology to deliver the bisphosphonate drug, Zoledronic acid, to prostate cancer cell lines as a potential to treating bone metastasis.

Chapter 1 - Thesis Introduction

1.1 Rationale

Up to 80% of patients with primary tumors of breast, prostate or lung will develop spine metastases (Maccauro et al., 2011). Spine metastases cause pain, functional deficit and severely diminished health related quality of life through fractures, vertebral instability and spinal cord and nerve-root compression. Currently spinal metastases are associated with high socioeconomic and healthcare costs and with advancements in medical, radiation and surgical oncology, these patients are living longer thereby increasing the disease burden (Falicov et al., 2006) (Wai et al., 2003). In current medical practice the gold standard of treatment for spinal metastases revolves around an extremely long and arduous journey for the patient. Treatment may include spinal tumor resection surgery, radiation therapy and/or chemotherapy (Rose, Clarke, & Dekutoski, 2011).

The urgency and importance associated with spinal metastases is due to the detrimental complications it can lead to. The vertebral column or axial spine consists of thirty-three vertebrae separated by cushioning intervertebral discs which are designed to provide stability and aid with the upright posture of humans (Kibler, Press, & Sciascia, 2006) (Humzah & Soames, 1988). Additionally, the forces applied to the spinal column are vast and include loading, torsion and shear forces. The column itself is divided into the vertebral body and vertebral arch which combine to form a vertebral foramen encasing the spinal cord. Once there are metastases, the morphology and properties of the bone alter leading to bone degradation and eventual pathological fractures. The pathological bone is weaker and more susceptible to complications for the patient. The metastases can infiltrate the bone to the extent where it collapses or fractures leading to severe pain and disability for the patient

(Yasuda et al., 1998). In addition to this, the tumor can actually expand in size, where it can compromise the spinal cord or exiting nerve roots leading to nerve deficit and possible paralysis (Schaberg & Gainor, 1985) (Maccauro et al., 2011).

With the detrimental outcomes of spine metastases being well known, treatment is usually conducted urgently and involves invasive measures. If the metastasis is resectable, major surgery is an early treatment option and this involves extensive surgical resection of the pathological bone (Walker, Yaszemski, Kim, Talac, & Currier, 2003) (Patchell et al., 2005). Surgical bone resection of metastatic tumors can lead to critical-size bone defects that do not self-repair. The void left behind is usually filled with bone graft obtained from the iliac crest of the patient which leads to significant patient morbidity due to pain and infection (Patchell et al., 2005). Following tumor resection, the spine can become unstable and this can delay patient recovery following surgery. It will lead to increased pain and limited activity permitted by the patient as instructed by their surgeon to ensure adequate healing. For this reason, continuous research is underway to establish a method to remove pathological bone, such as metastasis, and replace it with a compound or construct which increases stability and also aids the body in fighting the cancerous cells. Adjuncts commonly used with spine surgery are radiation therapy and chemotherapy (Santini et al., 2015). Not all cancer cell lines respond to these 2 adjuncts and there are substantial complications associated with both for the patient. Radiation therapy can lead to fatigue, generalized pain and skin dryness, thinning and increased infection rates following surgery (Hsiao, Daly, & Saligan, 2016) (Jereczek-Fossa, Marsiglia, & Orecchia, 2002) (Jereczek-Fossa, Marsiglia, & Orecchia, 2001). Chemotherapy has systemic effects and leads to fatigue, nausea, hair loss and numerous other side effects (Joly, Ahmed-Lecheheb, Thiery-Vuillemin,

Orillard, & Coquan, 2019). The important thing to note with these 2 adjuncts is that they are not focussed on diseased tissue. Chemotherapy is systemic in nature and affects healthy neighbouring cells.

Recently research has looked at the effect of antiresorptive medication such as bisphosphonates on bone metastases and tissue repair (Lipton, 2008) (Bobyn, McKenzie, Karabasz, Krygier, & Tanzer, 2009) (Miettinen et al., 2009). Bisphosphonates such as Zoledronic acid are historically used in osteoporosis (Black et al., 2007) (Reid et al., 2002) and Paget's disease management due to its osteoclast inhibiting capacity (Reid et al., 2005). Osteoclasts are a type of cell found in the bone which aid in bone resorption, a cell crucial for bone repair and regeneration. They do this by secreting collagenase which degrades protein and minerals in bone, a course described as bone resorption (Fleisch, 1998) (Rodan & Fleisch, 1996). Recent research has shown that bisphosphonate drugs at high doses have the ability to inhibit tumor induced bone resorption and pain accompanying this process. In addition to this, bisphosphonates have been shown to have anti-tumor and anti-angiogenic activity, opening the door to possible newer metastasis treatment therapies (Di Salvatore et al., 2011). Intravenous delivery of bisphosphonates is an option however it requires high does to have therapeutic effects. With the use of high doses however, there are systemic effects on the body and these risks include damage to the renal system, osteonecrosis of the jaw and ocular inflammation (Umunakwe, Herren, Kim, & Kohanim, 2017) (Selvaggi & Scagliotti, 2005). Oral administration of bisphosphonates is another option, but this does not allow adequate concentrations to reach the region of concern and is also associated with numerous side effects as described above.

Bone loss, instability and poor repair following tumor resection remains an unmet clinical need in the spine metastasis population (Patchell et al., 2005). Autologous bone graft and calcium phosphate bone substitutes are regularly used to increase stability of constructs following wide bony resections (Davarski et al., 2013). The mechanical advantage obtained using bone graft is clear and effective, but it has no anti-tumor effect. This is where more recent research has looked to nanotechnology. Nanotechnology is described as the alteration of matter with one or more dimension sized from 1 to 100 nanometers (Satalkar, Elger, & Shaw, 2016). It has numerous applications spanning from medicine, bioproducts and electronics. Within the realm of medicine, nanotechnology has been used to deliver drugs at a local level (Raj et al., 2019). This entails the coating of a specific drug on nanoparticles which can then be integrated to a specific area of interest. An example is nanobeads which can be engineered to have properties of interest such as the ability to carry a drug whilst being inert and safe for medical use (Kubackova, Zbytovska, & Holas, 2019). Nanotechnology is promising as a strategy for local delivery of drugs in various diseases and may help to advance the management of conditions such as spinal metastases.

1.2 Scope of The Project

This study investigated the use of nanotechnology in regard to drug delivery and spine metastasis management. The work conducted advances our knowledge of bisphosphonate action on spine metastasis, nanobead handling and drug loading and the delivery of bisphosphonates in vitro. The developments we have made take us closer to the ability of using nanotechnology to delivery anti-tumor drugs locally following tumor resection in spine metastasis patients. The methods highlighted in this study can also be expanded and used in other areas of medicine with other drug types. In

addition to this, the technology used can be integrated with current surgical methods to create advanced treatment goals for spinal metastasis patients.

1.3 Project Contributions to Healthcare

Modern medicine requires innovative approaches to create personalized devices that will enhance patient recovery. Following tumor resection in spine metastases, patients are left with large bony voids with limited local infiltration of anti-tumor drugs. Our study aims to advance our knowledge of bisphosphonate action, more specifically Zoledronate, on cancer cell lines that lead to spinal metastases. However, currently we are faced with difficulties of delivering drugs to the desired sites in a targeted manner. This research addresses this by looking at techniques to use nanotechnology to deliver drugs at the local region of the site of pathology. We foresee that our advancements will enable us to eventually produce personalized bone grafts to assist with bone healing and to reduce the risk of tumor recurrence. Local bone grafts which have anti-tumor effects are expected to accelerate patient recovery following spine tumor resection. They can be used to improve bone stability, and the local drug delivery will have combined analgesic and anti-tumor features. Our research may assist in the management of bone tumor patients in the future and has potential not only in treatments in spine surgery but also in other aspects of Orthopedic Surgery.

Current medicine is limited for patient management of spinal metastases and leaves patients with vast sequela (Joly et al., 2019) (Jereczek-Fossa et al., 2001). Drug delivery using nanotechnology is safe, reliable and relatively inexpensive (Kubackova et al., 2019). This study provides us with the

foundations to develop local drug delivery strategies within the realm of Orthopedic spine tumor patients following tumor resection.

Chapter 2 – Review of the Literature

2.1 Spine Metastasis

Tumors associated with the spine are extremely debilitating with ever increasing incidence as medical care and life expectancy continues to advance (Aebi, 2003). Spinal oncology can be separated into 2 groups; primary and secondary tumors of the spine. Primary tumors are unique as they originate from the spine itself. More commonly however, are secondary spine tumors which are tumors that originate from a different region in the body. The most common types of cancers which lead to spine metastases are; prostate, breast, lung, bladder and the thyroid gland, with 60 % arising from breast, lung and prostate cancer (Greenlee, Murray, Bolden, & Wingo, 2000) (Bartanusz & Porchet, 2003). Cadaveric studies have shown 30-90% of patients diagnosed with cancer have spinal metastases at their time of death (Sciubba et al., 2010).

The process in which cancer cells become metastatic is complex and involves multiple stages. It is important to note that the process will vary slightly dependant on the cell type in question, but they have been generally found to follow similar paths. The key feature of cancer cells that have the ability to metastasize is their ability to interact and reside in the microenvironment of the organ they have metastasized to, colonize, survive and proliferate (Croucher, McDonald, & Martin, 2016). The 'seed and soil' hypothesis was devised by Stephen Paget which refers to the concept that the bone acts as soil which houses the cancer cell which has seeded (Langley & Fidler, 2011). For cancer cells to metastasize they need to migrate to a new site. This usually occurs via a network such as the vasculature or the lymphatic system. Once it reaches the distant organ, it colonizes and adjust to its

new environment. At this point it is able to lie dormant for an extensive period of time (Ahangar, Aziz, Rosenzweig, & Weber, 2019). Following this dormancy, which can be an extensive time period, the cancer cell activates once more allowing the cell to proliferate. The final stage sees uncontrollable growth of the tumor. This will change the morphology of the bone it resides in, leading to complications associated with bone metastases such as pain, fractures and neurological compromize (Croucher et al., 2016) (Ahangar et al., 2019).

Current treatment for spinal metastases involves multidisciplinary involvement (Spratt et al., 2017). The primary surgical approach is extensive surgical excision of the pathological bone. Surgeons need to ensure all of the malignant cells are removed and for this reason they plan very wide resection margins. This extensive surgery can be supplemented with bone graft and instrumentation to aid in the stability of the bone (Patchell et al., 2005). On top of the general surgical risks such as infection, bleeding and injury to neurological structures, there is a high reoccurrence rate which might require further surgery (Sebaaly et al., 2018). Adjuncts to surgery include chemotherapy and radiotherapy which has proven beneficial in some, but not all cancer cell lines (Spratt et al., 2017).

2.2 Prostate Cancer Cell Lines

Prostate cancer continues to be the most common type of cancer diagnoses and the second highest cause of death from cancer in men (Yang et al., 2019). Prostate cancer metastasizes to bone very frequently and it has been shown that 91% of metastasis sites of stage 4 prostate cancer has been found in bone (Gandaglia et al., 2015). Patients who suffer from prostate cancer related metastasis

to bone endure a long course of medical sequelae and more than 50% will end up with skeletal related events such as fractures, which will reduce patient quality of life considerably (Luz & Aprikian, 2010).

Different cell lines exist for prostate cancer and the most common ones used in the field of research are LAPC4, LNCap, C42B, DU145 and PC3. As alluded to above, spinal metastases from primaries such as prostate cancer have a multidisciplinary treatment plan. Surgical excision, radiation therapy and chemotherapy are common management methods with current medical practice. Due to the systemic effects seen with anti-tumor drugs, research is looking at the possibility of delivering drugs locally to the area of interest and one drug class of interest is bisphosphonates. One study found autophagy of PC3, DU145, LNCaP with exposure to 100 µM of Zoledronic acid. Cell growth was inhibited and apoptosis increased with the administration of this drug, suggesting Zoledronic acid inhibits prostate cancer by apoptosis and autophagy (J. F. Lin et al., 2011). Another study found higher concentrations of Zoledronic acid affected proliferation and apoptosis of PC3 and LNCap prostate cancer cell lines. They tested the following concentrations; 0.25, 0.5, 1, 3, 5 or 10 µM and found reduced proliferation with the higher concentrations, which was confirmed by reversing and enhancing the effect of Zoledronic acid on cell proliferation with caspase 3, 7 or survivin siRNA (Almubarak et al., 2011). A further study found PC3 prostate cancer cell lines treated with various Zoledronic acid concentrations showed low concentrations enhance the inflammatory profile and acts to aid survival signals for the PC3 cells in comparison to the higher concentrations (Y.-C. Lin et al., 2014). Finally a study looking at 100 µM of Zoledronic acid for 48 hours found various prostate cancer cells had inhibited cell growth (Nogawa et al., 2005).

2.3 Bisphosphonate drug, Zoledronic acid

Bisphosphonate drugs are stable analogues of the inorganic Pyrophosphates (PPI) (Widler, Jahnke, & Green, 2012). PPI is found naturally in the body and it acts by inhibiting calcification due to its interaction with hydroxyapatite and it also prevents the dissolution of hydroxyapatite (Drake, Clarke, & Khosla, 2008). These features were thought to be important initially for conditions such as osteoporosis but PPI is unstable prior to oxygen bridging. With the oxygen bridge being converted to a carbon bridge, a stable analogue of PPI was formed and termed bisphosphonate (Fig. 1) (Russell & Rogers, 1999). This compound actively targets osteoclast cells which are the cells that cause bone resorption in the body (Ibrahim et al., 2003). For this reason, their main use in modern medicine has been in conditions with abnormal bone homeostasis resulting in underossification such as osteoporosis and Paget's disease (Black et al., 2007) (Reid et al., 2002). Furthermore, bisphosphonates were found to have anti-tumor effects. They have been found to be able to induce tumor apoptosis, inhibit cell adhesion, invasion and proliferation, thus reducing tumor count (Teixeira, Branco, Fernandes, & Costa-Rodrigues, 2019).

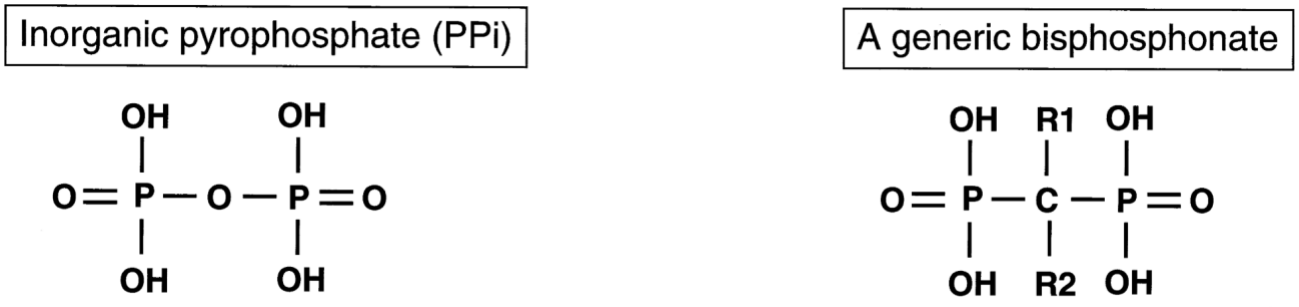

Figure 1. An illustration showing how the oxygen bridge is converted to a carbon bridge stabilizing the PPI to a generic Bisphosphonate (Russell & Rogers, 1999).

Zoledronic acid is a type of third generation nitrogen containing bisphosphonate drug and has been found to be one of the most effective bisphosphonates (Akoury et al., 2019). Zoledronic acid has been proven to reduce osteoclast mediated bone resorption seen in bone metastasis. In addition to this, evidence shows that it aids in reducing the progression of bone metastasis from various primaries such as prostate, lung and breast cancer (Reuben et al., 2011). When used in a patient with skeletal pain due to bone metastases it has also been found to reduce this pain experienced by patients and improve their quality of life (Saad et al., 2002).

Extensive research has been conducted to understand the action of Zoledronic acid. The mechanism is not clear but it has been found to aid in tumor apoptosis, guiding the immune system in its action against tumor cells, inhibiting the invasion of tumor cells, reduce tumor angiogenesis and proliferation (Senaratne, Pirianov, Mansi, Arnett, & Colston, 2000). It is well known that this drug can be delivered intravenously or orally, but these methods have both been shown to have complications. One issue is the inability to achieve a large enough dose of the drug in the area of interest as the drug is spread systemically. Secondly, due to the systemic effects, higher doses have to be used which create multiple complications such as gastrointestinal irritation, ocular inflammation and osteonecrosis of the jaw (Umunakwe et al., 2017) (Selvaggi & Scagliotti, 2005).

To resolve the issue of having to use high doses of systemic Zoledronic acid, research is being conducted to devise a method of local delivery of the drug. Zoledronic acid has been implemented in animal studies looking at its local delivery using implants which were found to help with bone

remodelling (Bobyn et al., 2009) (Miettinen et al., 2009). Our group has previously shown that the local delivery of Zoledronic acid using a catheter inserted into the affected bone in mice led to reduced tumor proliferation, increased tumor apoptosis and lowered tumor induced osteolysis by tumor cells (Nooh et al., 2017). Furthermore, another study performed by our group showed that the action of low dose Zoledronic acid (3-10 μM) on prostate cancer cell lines and spine metastases secondary to prostate cancer decreased cell proliferation. The same doses were also found to inhibit tumor cell migration and 3D cell growth invasion making Zoledronic acid a great contender of being the local drug to tackle bone metastases following tumour resection (Akoury et al., 2019).

2.4 Nanotechnology, Nanobeads

Nanotechnology has allowed the development of nanoparticles which are described to be less than 100 nanometers in at least 1 dimension (Satalkar et al., 2016). Figure 2 illustrates the size of nanoparticles in relation with other matter to conceptualize this better (Wilczewska, Niemirowicz, Markiewicz, & Car, 2012). A lot of research is being conducted to utilize this technology for biomedical applications. The common goal has been to create nanocarriers which are able to transport bioactive chemicals such as drugs in the human body (Suri, Fenniri, & Singh, 2007). Different compounds being used currently for this purpose span from liposomes, lipids, nanoparticles, silicon, dendrites or carbon materials (Wilczewska et al., 2012).

Established drug delivery consists of systemic or oral routes which have been shown to have limited activity and generalizability in terms of target action. With nanotechnology, particles can be formed which lead to controlled and local drug delivery. This means that the drug is delivered to the region

of interest, reducing the unwanted side effects on neighbouring healthy cells. Furthermore, this method allows slower and more concentrated release of a drug to tissues and thus lower concentrations can be used which means safer drug administration (Nevozhay, Kanska, Budzynska, & Boratynski, 2007).

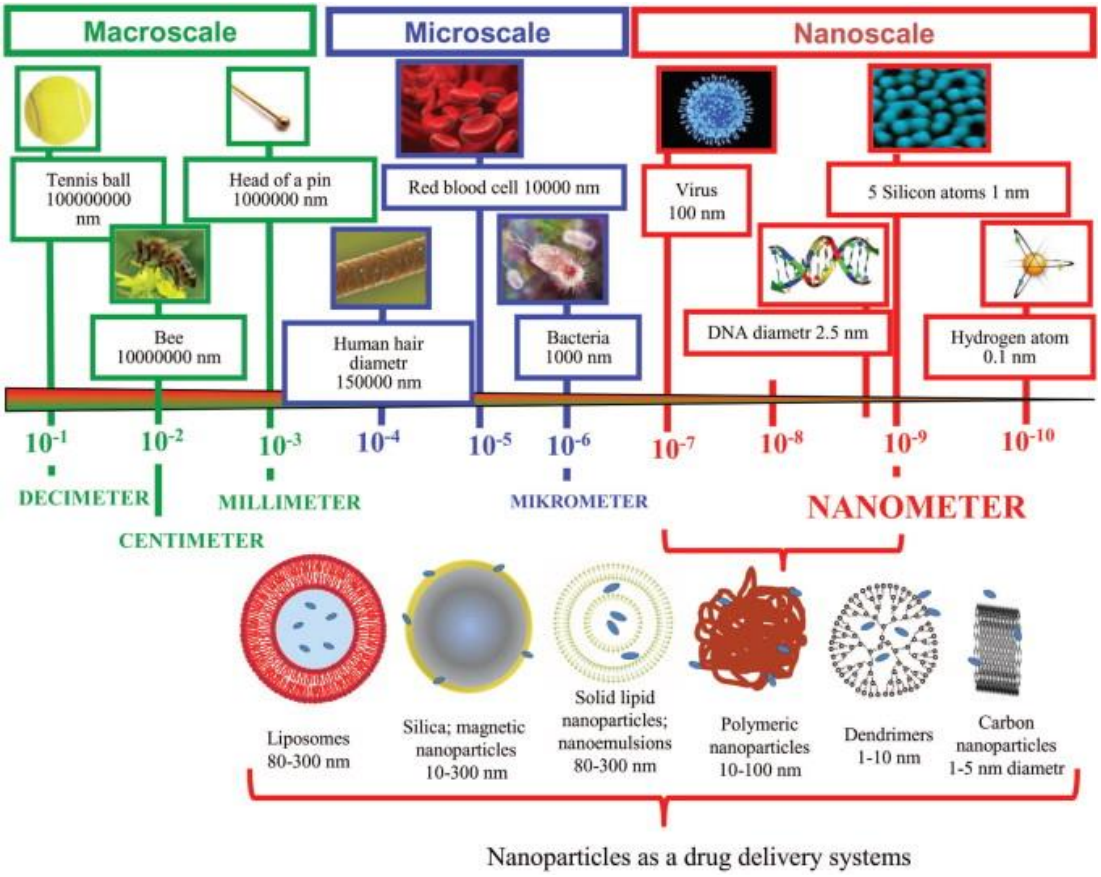

Fig 2. Illustration showing the comparison of difference size matters to better conceptualize the size of nanoparticles *(Wilczewska et al., 2012).*

An important part of drug delivery using nanocarriers is the method in which the drug is bound to the nanoparticles. A drug can be adsorbed or bounded to the carrier using covalent bonds. The latter

method has been found to be better as it allows complete control of the drug concentration attached to the carrier (Di Pasqua, Wallner, Kerwood, & Dabrowiak, 2009). The carriers can then be made so as to be actively attracted to the target site by using recognition ligands which bind to conjugate antibodies or it can be done passively through permeable tissues (Nevozhay et al., 2007). Drugs have then been seen to release low doses in an attempt to create an equilibrium with its new environment.

Recent advances have been made using silica materials to deliver drugs in a controlled matter. The different types of silica materials used currently are; mesoporous silica nanoparticles, xerogels and SBA-15 (Santa Barbara University mesoporous silica material) (Wei, Hu, & Zhang, 2010) (Czarnobaj, 2008). Silica based nanoparticles are commonly being used due to their benefits of being easy to use, biocompatible and their extremely porous structure. These features make it an ideal compound to use for the safe and local delivery of a drug. The method of loading silica particles with a drug involves adsorption (Di Pasqua et al., 2009). The drug is subsequently delivered to the target tissue or cells via diffusion at a steady state (Li, Su, Cheng, & Deng, 2010). Examples of drugs that have been adsorbed onto nanoparticles include, anti-cancer drugs such as carboplatin (Di Pasqua et al., 2009), antibiotics (Li et al., 2010) and hypertensive medication (Popovici, Seftel, Mihai, Popovici, & Voicu, 2011).

A lot of work is still required to produce nanoparticles that are fully functional. With local delivery of a drug there are aspects that still need to be tested thoroughly. These include toxicity to neighbouring healthy cells and methods to bind the drug on the particles effectively ensuring the drug is released over a certain time period.

2.5 Bioprinting

3D printing of biological materials is a form of additive manufacturing; it is a fairly new but quickly developing technique. It is a method to produce constructs with a high level of control over the spatial distribution of biological materials , using a model generated on a computer (McHugh et al., 2017). The key thing is that it allows the formation of complicated structures which would otherwise be overtly difficult to make using conventional methods. Bioprinting is a form of additive manufacturing where cells are seeded in a confined area in 3D space (Wang et al., 2018). This technology can be used in various in-vitro settings checking disease modelling, drug testing and also enabling the formation of implantable tissue such as cartilage (Gao, Hubbell, Schilling, Dai, & Cui, 2017) or bone (Zhou et al., 2016).

Bioprinting works by suspending cells in a bioink and then extruding this through a nozzle on a targeted region. A surface such as a well is calibrated for the nozzle to act on and the bioprinter can be coded to produce a specific 3D model using the loaded bioink (Ghidini, 2018). This method has been found to lessen stress experienced by cells due to the high resolution and lack of forced cell extrusion. Another method is for the printer to drop the bioink forming fibers (Cui & Boland, 2009). Prior to the next layer being added, the cells are crosslinked ensuring a 3D structure can be formed. The gel that the cells are suspended in allows for smooth and safe transfer of the cells.

The future of bioprinting is the fact that it allows in-vitro assessment of tissues. The formation of complicated 3D models using this type of printer permits us to form organoids or units of various organ systems to look at their disease progression and to test the application of various treatments.

Studies have shown the advantages of testing cells in 3D structure as oppose to a 2D in terms of assessing cell activity, with higher accuracy found in the 3D models (Riedl et al., 2017). Bioprinting makes scalability and reproducibility extremely easy and efficient. It helps us create environments which represent environments found in the human body and thus provides the capacity for us to create different lifelike treatments (Mathews Griner et al., 2016). To date, different studies have created models representing skeletal muscle (Kim et al., 2018), cardiac cells (Zhang et al., 2016), kidney and skin (Pourchet et al., 2017) which has made experimentation on these tissue types easier and more realistic. Limitations associated with bioprinting come from the bioink formed. An appropriate viscosity must be achieved, as too high a viscosity will require very high extrusion pressures and if it is too low, the structure will collapse during its formation (Gungor-Ozkerim, Inci, Zhang, Khademhosseini, & Dokmeci, 2018).

Chapter 3 – The Use of Nanobead Technology to Deliver Zoledronic Acid to Prostate Cancer Cell Lines

3.1 Objectives and Hypothesis

Bone metastases continue to be a great cause of patient morbidity due to cancer related musculoskeletal pain and fractures. Patient quality of life is severely diminished and is difficult to recover from (Yasuda et al., 1998). Current medical practice involves surgical resection, radiation therapy and chemotherapy (Rose et al., 2011). Surgical resection is invasive and typically leads to instability of the spine. In addition to this, some cancer cells might still be present in the region of interest following resection (Falicov et al., 2006).

In our study we aimed to develop a carrier to deliver an anti-tumor drug locally to affect prostate cancer cell lines with high metastatic ability. Our objectives were: Load silica beads with Zoledronic Acid, test its release, test effects in 2D prostate cancer model, and test effects in 3D bioprinted prostate cancer model.

We hypothesize that silica nanobeads with bisphosphonate, Zoledronic acid, will limit prostate cancer proliferation and migration. We foresee that we will be able to create a 3D model which will show gradual and local release of this drug in a controlled environment. The aim of this work is to incorporate these loaded nanobeads in different environments representing spine metastases from prostate cancer cell lines.

3.2 Introduction

Spine metastasis has detrimental effects on patient quality of life and continuous research is underway to discover the best treatment plan for these cases. Spine surgery involves large tumor resections which lead to large bone defects and instability of the spine (Falicov et al., 2006). In addition to this, tumor recurrence is common (Sebaaly et al., 2018) and advancements in management are needed to reduce this risk. With current practice, patients are started on multiple treatment plans including radiation therapy, chemotherapy and also bisphosphonate drugs (Spratt et al., 2017). These methods have shown great effect in reducing tumor size and lowering recurrence rate, but their systemic application means high complications and side effects associated with their administration. They are commonly associated with gastrointestinal symptoms, generalized fatigue and osteonecrosis of the jaw with bisphosphonate drugs specifically (Umunakwe et al., 2017) (Selvaggi & Scagliotti, 2005). Current attempts are being made to overcome these side effects by lowering the dose of the drugs administered which is enabled by locally delivery the drug. For this to be feasible, a carrier will need to transmit the drug to the region affected and this needs to be a gradual release so healthy surrounding tissues are not damaged.

Advances are being made in creating different delivery methods of drugs. More recent interests have come in the use of nanotechnology as the main carrier for this purpose (Wilczewska et al., 2012). Nanotechnology gives the user flexibility of loading the carrier with the required dose and also permits gradual release of the drug. Previous studies in our laboratory have shown the effects of local delivery of the bisphosphonate drug, Zoledronic acid, to reduce proliferation and migration of cancer cells (Akoury et al., 2019). We attempt to replicate these results in a 3D bioprinted model where silica

nanobeads will be the carrier of Zoledronic acid in a prostate cancer bioprinted model to show that Zoledronic acid can be delivered safely, gradually and to the same or better effect as previous studies.

3.3 Methods

3.3.1 Preparing Phosphate Buffered Saline (PBS)

PBS was prepared using 1 bag of D5652-1L powder which was mixed with 1 litre of molecular water. It was stirred until the contents of the cylinder were dissolved (approximately 5 minutes). Suction the liquid formed gradually 500 ml at a time through a filter. Once 500 ml has been filtered through, it is poured into a sterile bottle, seal it and label it accordingly before placing it in the fridge at 4°C.

3.3.2 Preparing **Roswell Park Memorial Institute (*RPMI) Medium***

RPMI was prepared by first warming; fetal bovine serum (FBS), RPMI and antibiotic (penicillin/streptomycin) in a water bath set at 37°C. After this, the FBS was placed in a 56°C water bath for 30 minutes to inactivate certain proteins and following this, the solution was cooled in room temperature for 20 minutes. 500 ml of RPMI was placed in a bottle with 50 ml of FBS and 5 ml of the antibiotic solution. The bottle was then capped, sealed and placed in a fridge at 4°C.

3.3.3 Thawing cancer cells

Cells that had previously been placed in liquid nitrogen were thawed appropriately prior to utilization. The cells were obtained from the liquid nitrogen tank. The frozen cells were thawed quickly in a water bath at 37°C and whilst this was defrosting, 9 ml of fresh media was placed in a measuring tube. Following this, 1 ml of the now defrosted solution with cells were placed in that same tube making a

total of 10 ml. This tube was then centrifuged at 1500 RPM for 5 minutes. After the centrifuge process, the cells formed a pellet at the bottom of the tube. The media was then aspirated off the top of the cells, with care not to suction the pellet of cells itself. 2 ml of media was then added to the cells and mixed well. A sterile flask containing 8 ml of media was then used to house the 2 ml of media and cells forming a 10 ml flask with cells and media. The flask was then gently rocked manually to evenly distribute the cells on the bottom of the flask. Cells were cultured in a humidified incubator at 37 C and 5% CO_2, media was changed twice a week.

3.3.4 Cell Passaging

The cells that were to be passaged were taken and rinsed using 3 ml of PBS (D565210X1L, Sigma Aldrich). The flask was rocked manually to ensure all of the cells were washed. The PBS solution was discarded and then 2 ml of trypsin-edta 0.25% was added. The flask was then placed in the incubator for 10 minutes to allow trypsinization of the cells. Following this, the cell detachment was checkec using a microscope. The trypsin was then deactivated by adding 7 ml of medium (RPMI 11835-030 Gibco) to the flask. The cells in the medium were then centrifuge at 1500 RPM for 5 minutes. Following this, the media was removed above the pellet. 8 ml of media was placed in 2 new flasks. Then 4 ml of media was placed in the tube with cells and mixed well. Then 2 ml was taken from the cell mixture and placed in each flask containing 8 ml of media already. The flasks were then rocked to ensure spread of the cells and adherence to the bottom of the flasks. The flasks were then labelled, sealed and placed in the incubator.

3.3.5 Cell Freezing

Please refer to. ‘3.3.4 Cell Passaging’ up until the cells being detached and prior to centrifuging. At this point 2 ml of cell culture freezing medium (12648/010 Gibco) was added to the tube and cells were mixed well in this solution. Then 1 ml of this solution was transferred to 2 cryotubes (Sarstedt 72.380.002) each and were then labelled. Following this, the cryotubes were placed in a -80°C freezer for approximately 2 days before transferring them to a liquid nitrogen tank for long term storage.

3.3.6 Cell Counting

Please refer to. ‘3.3.4 Cell Passaging’ up until the cells have been centrifuged and are in pellet form at the bottom of the tube. Following this, 3 ml of media was added, and the cells mixed. Before applying these cells to the next step, the hemocytometer (Fisher 0267110) with its cover slide was prepared. A 24 well plate was obtained and 90 µL of Trypan blue (T8154) was placed in a single well. 30 µL from the cell/medium mixture was placed into the well with Trypan blue. Following this, 10 µL of the 120 µL solution was placed on the hemocytometer directly under the cover slide which sits on top of the hemocytometer. Following this, the cells on the hemocytometer were visualized under the microscope. Under the microscopy 4 quadrants were seen (Figure. 3) and each one of these quadrants contain 16 small squares which represent the total area of the quadrant.

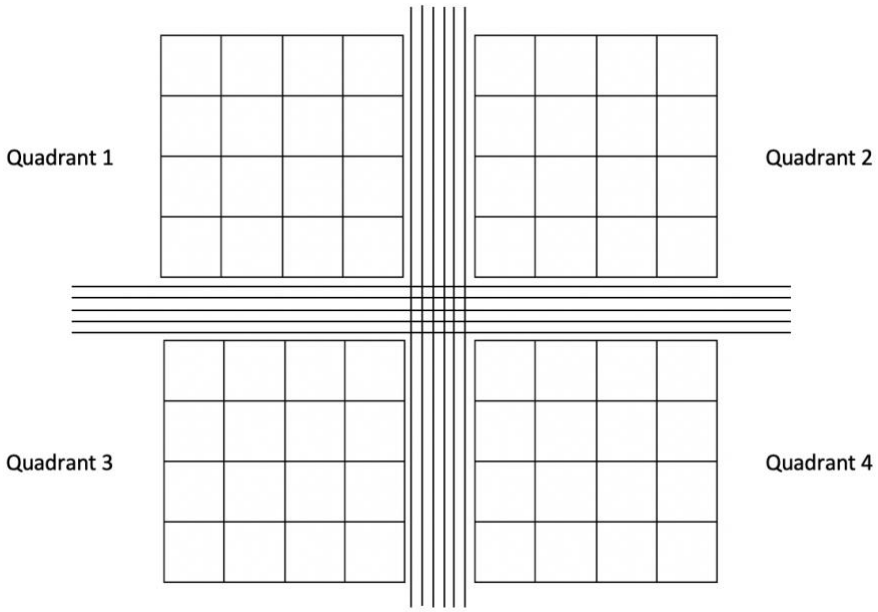

Figure 3. Illustration showing the hemochromocytometer highlighting the 4 quadrants where cell counting must be done.

All of the cells in each quadrant were counted separately using a counting device to limit errors. Cells in each quadrant were noted down and recorded. Once the cells in each of the 4 quadrants had been calculated, the total number of cells in the quadrant were added together and divided by 100 and multiplied by the volume of solution the cells were dispensed in. The final value was the number obtained x 10^6 in the volume of solution the cells were dispensed in (for example 3 ml in our experiment). After the cell counting was done, it was possible to calculate how many cells will be in a set volume of solution containing the cells to conduct controlled experiments.

3.3.7 Proliferation Assay

Proliferation was assessed using both Alamarblue® kit (USA, Thermofisher — cat DAL1025) and Vybrant® MTT cell proliferation kit (USA, Thermofisher—cat V13154) according to the protocols

provided by the manufacturers. The prostate cancer cell lines (PC3, 22RV1 and LAPC4) were seeded at a density of 5000 cells/well in 96 well plates (USA, Costar, FisherScientific—cat 3882) coated with poly-L-lysine (USA, Sigma — cat P4707-50ML) and were grown in standard media (RPMI, 10% FBS, 1% PS) for 24 hours. After 24 hours, cells were treated with vehicle (PBS1x) or Zoledronic acid (USA, Sigma — cat SML0223-50MG) in low-serum conditions (1% FBS) for a total of 7 days. The media was replaced was then replaced on day 4 for each experiment. For the Alamarblue® assay, the dye was added to the media at 1:10 dilution on day 7 and cells were incubated at 37 °C for 4 hours. For Vybrant® MTT cell proliferation assay, the cells were labelled with MTT at 1:10 dilution on day 7 and incubated for a total of 4 hours at 37 °C. After this, 75 µl of media containing MTT was removed from each well and then 50 µl of DMSO (USA, Sigma – cat D2438) was added to each well and then incubated for 10 min at 37 °C. After incubation, the fluorescence of Alamarblue (Excitation — 540 nm, Emission 585) or the absorbance of MTT (540 nm) were analyzed using the Infinite Tecan M200 Pro microplate reader (Tecan Trading AG, Männedorf, Switzerland). (Modified from method performed by my group, (Akoury et al., 2019))

3.3.8 Migration Assay

To analyze migration of the LAPC4 cell lines they were seeded at a density of 20,000 cells/well in the upper compartment of Falcon™ cell culture inserts (8 µm pore size; Canada, Falcon — cat 353097) coated with poly-L-lysine. The next day, LAPC4 were treated with vehicle or Zoledronic acid at different concentrations with 1% FBS. Cell migration was assessed for 7 days with the use of vehicle or RPMI combined with drug supplemented with 2% FBS media as a chemoattractant below the insert. After migration through the filter, the cells of both compartments were assayed for alamarblue

to check for cell proliferation. The cells of the upper compartment of the insert were then removed using cotton swabs, and those on the lower compartment were fixed with 4% paraformaldehyde (USA, Thermofisher—cat 28908), counterstained with DAPI (USA, Sigma—cat F6057-20ML) and imaged using an inverted microscope (USA, Olympus, IX71). After this step the cells were then counted. 5 or more random fields were used to do the cell counting and this was done 3 times each. (Akoury et al., 2019)).

3.3.9 Scratch Assay

The plates used were initially coated with collagen. 500 µL of collagen at 3 mg/ml were placed in each well of the 24 well plate. Incubated for 2 hours at 37 °C and then the wells were rinsed x 2 with 1 ml of PBS. The plates were allowed to dry in the cell culture hood before performing the next step. The 24 well plate was turned upside down and 3 horizontal lines were drawn equidistant from each other in each row using different colours for easy identification later. After performing a cell count, 80,000 cells were placed per well and 500 µL of medium was placed on top. These cells were allowed to adhere by placing the plate in the incubator for 24 hours. After cell adherence, a vertical scratch was made in each well using a 200 µL pipette tip. A ruler was used to aid with this part to ensure higher accuracy. The pipette tip was replaced after 4 scratches to ensure a sharp pipette tip was used consistently. The wells were then washed with RPMI to remove any dead cells that were scratched off. Vehicle or Zoledronic acid at different concentrations in low-serum conditions (1% FBS) were placed in each well in triplicates of 4. Each day the plate was placed under the microscope and a photo taken to assess the migration of the cells. The images were then analyzed using image J (See 3.3.10 Image J Analysis) to assess the area encompassed by the cells.

3.3.10 Image J Analysis

Image J is an open source application written by Java (https://imagej.nih.gov/ij/index.html) used to analyze the cell migration in the scratch assay experiments. Each image taken from the scratch assay per day, per well were uploaded onto the program. Using the lasso tool to manually draw around the cells was done to assess amount of migration. This allowed calculation of the total area of cells covered in the well and it allowed comparison of the area the cells cover with each condition after each day of treatment. Using statistical analysis of ANOVA we were able to compare the area difference between each day of each condition per well.

3.3.11 3D Osteoblast Model

This experiment was designed to assess stem cell conversion to osteoblast activity using a 3D model. 3 different variables were performed; agarose, agarose + collagen, agarose + collagen + hydroxyapatite (ID 677418). Variables were made in 25 ml tubes. Tube 1 was made with 0.5% agarose and 10,000 stem cells introduced to the agarose. Tube 2 was 0.5% agarose + collagen combined with the same number of stem cells. Tube 3 was 0.5% agarose + collagen + hydroxyapatite combined with 10,000 stem cells. These were then placed in triplicates in 2 different plates. After 24 hours, each variable was placed in 2 different settings 1) control media DMEM and 2) osteogenic media. The media was changed accordingly every 3 days and the experiment was run for 21 days. Following this, live Dead Viability / Cytotoxicity Assay was performed (see 3.3.16 Live Dead Viability / Cytotoxicity Assay).

3.3.12 Live Dead Viability / Cytotoxicity Assay

Live/Dead® viability/cytotoxicity assay was performed as previously described by my laboratory (Akoury et al., 2019). A punch biopsy from the 3D model made in 3.3.13 was taken. 500 µl glycerol (G9012, Sigma-Aldrich) and 4.5 ml DMEM solution (5ml solution) was placed in a tube. Buffer; 3 mcL of calcein + 9mcL of ethidium homodimer was then added to this. Then the biopsy was added to the well with the above solution. 100 µl of live/dead mix (2 µM calcein AM and 4 µM ethidium homodimer-1 (EthD-1) diluted in 1 ml PBS1x) (USA, Themofisher — cat L3224) was then added to each well. Following this, the cells were incubated at room temperature for 40 min. Then using an inverted fluorescence microscope (USA, Olympus, IX71) the cells were counted. Live cells were labelled green (calcein AM) and dead cells were stained red (EthD-1).

3.3.13 Chitosan Preparation

0.11M HCl was first made by adding 430 µl of concentrated HCl to 10 ml of distilled H_20 in a 50 ml measuring cylinder. The cylinder was then filled up to 50 ml with distilled water. 25 ml of that solution was then taken and 0.125 g of chitosan (44887750G, Sigma) was added to make 1% chitosan. This composition was then mixed thoroughly using a high-speed vortex for 10 minutes.

3.3.14 Nanobead Preparation

10 mg of nanobeads (Aldrich – 805890-1G – Lot # MKBW7532V – Silica, mesoporous 0.5 µm particle size, pore size of -2 nm) were placed in a 15 ml scintillation tube. 1 ml of PBS was added to this and the tube placed in a sonicating bath for 30 minutes. Following 30 minutes of sonication, the tubes were split into 2 scintillation tubes (500 µl in each) and 500 µl of PBS were added to each vial (making

2 tubes of 1 ml). In vial 1: 20 µl of chitosan (3.3.15 Chitosan Preparation) was added and vial 2: 20 µl of 0.11M HCl was added. 1 mM of Fluorescent Zoledronate (Fam-Zol) was added to each tube and magnetic bars placed in each tube. The tubes were covered with foil as the Fam-Zol is light sensitive. The tubes were incubate for 24 hours at room temperature on a magnetic stirrer. Following this, both tubes were transferred to separate Eppendorf tubes and the beads were spun down (3 minutes at 11500 RPM). Supernatant was removed off and stored at -20°C as this was the unbound Fam-Zol. The beads were then washed with 600 µl of PBS X 3 and re-suspended in 600 µl of PBS. The beads were then ready to test release of Fam-Zol (See 3.3.17 Nanobead Fam-Zol Experiments).

3.3.15 Nanobead Fam-Zol Experiments

Nanobeads were prepared with Fam-Zol as per *'3.3.16 Nanobead Preparation'.* For the following experiments, nanobeads with and without chitosan were prepared in triplicate. 3 different experiments were performed: Fam-Zol release from nanobeads, Fam-Zol absorption by bone putty from nanobeads, bone putty/Fam-Zol mixture release of Fam-Zol.

3.3.15.1 Nanobead Fam-Zol Release

Prepared nanobead/Fam-Zol was placed in PBS solution as illustrated in Figure 5. 250 µl of PBS/nanobead mixture was added to an Eppendorf tube. 500 µl of PBS was added on top (total of 750 µl solution). Every 24 hours 250 µl was removed and stored at -20°C and the Eppendorf tube was resuspended with original 250 µl PBS. The stored PBS removed at each 24 is then analyzed using the Infinite Tecan M200 Pro microplate reader (Tecan Trading AG, Männedorf, Switzerland).

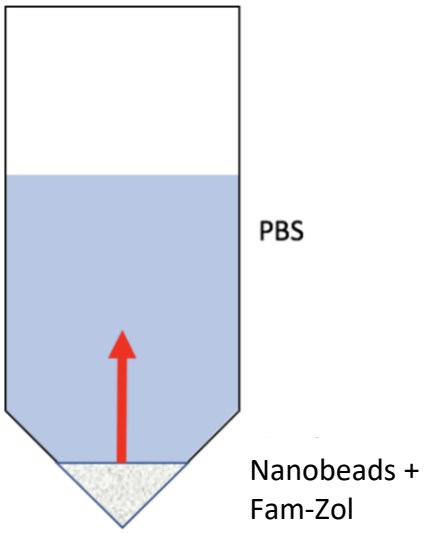

Figure 5. Illustration depicting the Eppendorf tube with the Fam-Zol coated nanobeads placed in PBS for the experiment.

3.3.15.2 Fam-Zol absorption by bone putty from nanobeads

0.1 g of bone putty was placed in bottom of an Eppendorf tube. Add 500 µl of PBS/nanobead mixture on top of putty as demonstrated on Figure 6. Every 24 hours 250 µl of solution was removed and stored at -20°C and then 250 µl PBS was resuspended in the Eppendorf tube. The stored PBS removed at each 24 hours is then analyzed using the Infinite Tecan M200 Pro microplate reader (Tecan Trading AG, Männedorf, Switzerland).

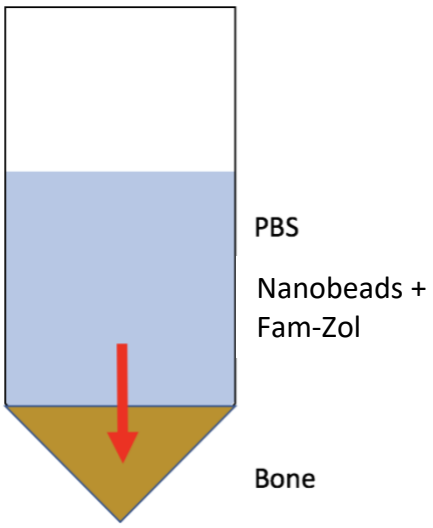

Figure 6. Illustration depicting the Eppendorf tube with the Fam-Zol coated nanobeads placed in PBS above bone putty for the experiment.

3.3.15.3 Bone putty/Fam-Zol mixture release of Fam-Zol

0.1 g of bone putty was placed in the Eppendorf tube. 250 µl of PBS/nanobead mixture was added and mix thoroughly with bone putty. Following this, 500 µl of PBS was added on top of the composite as demonstrated in Figure 7. Every 24 hours 250 µl was removed and stored at -20°C. Then, 250 µl PBS was resuspended in the Eppendorf tube. The stored PBS removed at each 24 hours was then analyzed using the Infinite Tecan M200 Pro microplate reader (Tecan Trading AG, Männedorf, Switzerland).

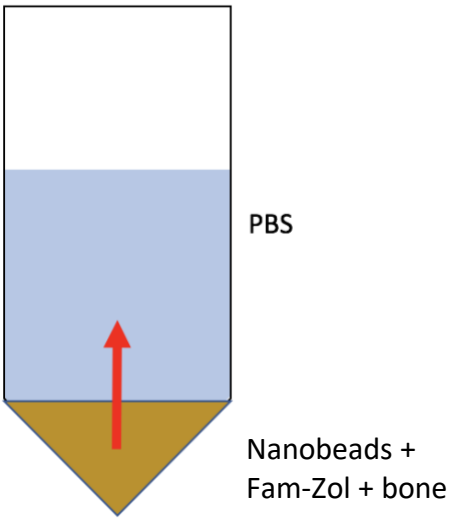

Figure 7. Illustration depicting the Eppendorf tube with the Fam-Zol coated nanobeads mixed in with the bone putty checking its release into the PBS above as for the experiment.

The experiments were run for 14 days and supernatant from each day was analyzed using the Infinite Tecan M200 Pro microplate reader (Tecan Trading AG, Männedorf, Switzerland) with the following settings: Wavelength = 540 nm, # flashes = 25, gain = 60.

3.3.17 Bioprinting and 3D model construction

For preparing the bioink, 1.2 g of sodium alginate (Protanal LF 10/60 FT, FMC BioPolymer) was mixed with 2.8 g of gelatin (G9391, Sigma) in 40 ml of sterile PBS (inside a sterile beaker with a stirring rod) to create a final concentration of 3% alginate and 7% gelatin. This mixture was incubated at 37 °C on a magnetic stirrer for 3 hours to ensure homogeneous mixing. Following this, the gel was placed inside a 50 ml sterile tube, capped and sealed with parafilm. Next, it was centrifuged at 3000 RPM for 5 minutes to remove any air bubbles. The sealed bottle was then placed under ultraviolet light for 24 hours to sterilize the bioink. Prior to usage of the gel, it was reheated in a 37 °C water bath for 30 minutes to reduce the viscosity such that it was suitable for cell mixing and bioprinting.

C42B cells were counted according to section '3.3.6 Cell Counting'. A 3 million cell pellet was isolated in a 50 ml tube and media was discarded. Next, the pellet was suspended in 3 ml of preheated bioink gel to achieve a final concentration of 1 million cells per 1 ml of gel. Following this, the gel/cell mixture were loaded into sterile printing cartridges (3 ml) in the sterile fume hood for bioprinting. Cartridges were sterilized by cleaning them with 70% ethanol and leaving them under ultraviolet light for 3 hours.

3D models for bioprinting were created using the modelling program SketchUp Pro 2018 (Version 18.0.16975). The model had dimensions of 10 mm diameter and 1.5 mm thickness. The model was exported as a Stereolithography (.stl) file and uploaded on the pneumatic bioprinter (CELLINK BIO X). Bioink cartridges were loaded into the bioprinter and the model was printed into sterile 24 well plates. Once models were printed, each gels disc was crosslinked using calcium chloride (100 mM) for 10

minutes at which point the calcium chloride was discarded and replaced with 500 ml of 10% supplemented DMEM media and incubated at 37 °C for 24 hours.

Nanobeads were prepared as per '3.3.16 Nanobead Preparation' on the same day the models were bioprinted. Our goal was to load the nanobeads with the same dose of Zoledronate (10 µl) that our group has shown to achieve the desired reduction in metabolic activity of prostate cancer cells(Akoury et al., 2019). Given the release kinetics of Fam-Zol from nanobeads (approximately one-third of loaded drug over 7 days) (Section 3.3.17) we decided to investigate a range of Zoledronate loading doses to encompass the 10 µM therapeutic dose in a 1 ml culture environment (290.1 ng). Thus, using the same protocol, nanobeads were loaded with the following Zoledronate doses; 1/2x, 1x, 5x, 10x and 100x (1x = 290.1 ng which is equivalent to 10 µM in 1 ml of media). Thus after 24 hours, both the nanobeads and models were ready to be combined. The 24 well plates with the models inside had their media discarded in order to allow punching a 4 mm hole in the center of each gel using a sterile 4 mm biopsy punch. Next, prewarmed un-crosslinked gel was deposited in the void created using the punch biopsy. Following this, 6 µl of nanobead/PBS suspension was carefully deposited within the center of the aqueous gel just placed in the center of the model previously. Next, the aqueous central portion was crosslinked using calcium chloride in order to create a homogenous model with drug loaded nanobeads suspended in the center of the model as seen on Figure 8. Each variable tested (nanobeads only, 1/2x, 1x, 5x, 10x and 100x) was performed in triplicates and this experiment was conducted 3 independent times to achieve an n=3. Concurrently intact separate models which were not punched (Fig 9a), were treated directly using the same variables as the

nanobeads were loaded with. All wells were filled with 1 ml of 1% serum DMEM and incubated for 7 days at 37 °C, without any media change throughout this period.

Following 7 days of incubation, the media was discarded and replaced with 450 µl of fresh 1% serum DMEM and 50 µl of alamarblue to achieve a 10% concentration. The models were then inspected under the microscope to check the cells within the gel (Fig 9). This was then incubated for 4 hours at 37 °C. Following this, the plates were observed for colour change from blue to pink and analyzed using the TECAN machine as per protocol 3.3.7 MTT.

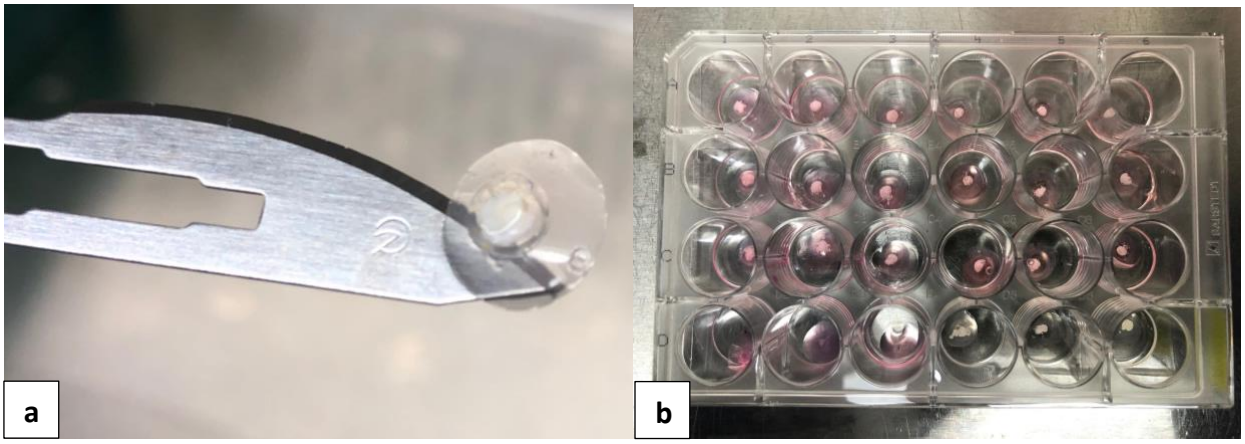

Figure 8. a) Photograph illustrating the 3D model created by placing Zoledronate coated nanobeads in the center of a 3D bioprinted C42B prostate cancer cell disc. B) Photograph illustrating the 24 well plate with the 3D bioprinted model ready for experimentation.

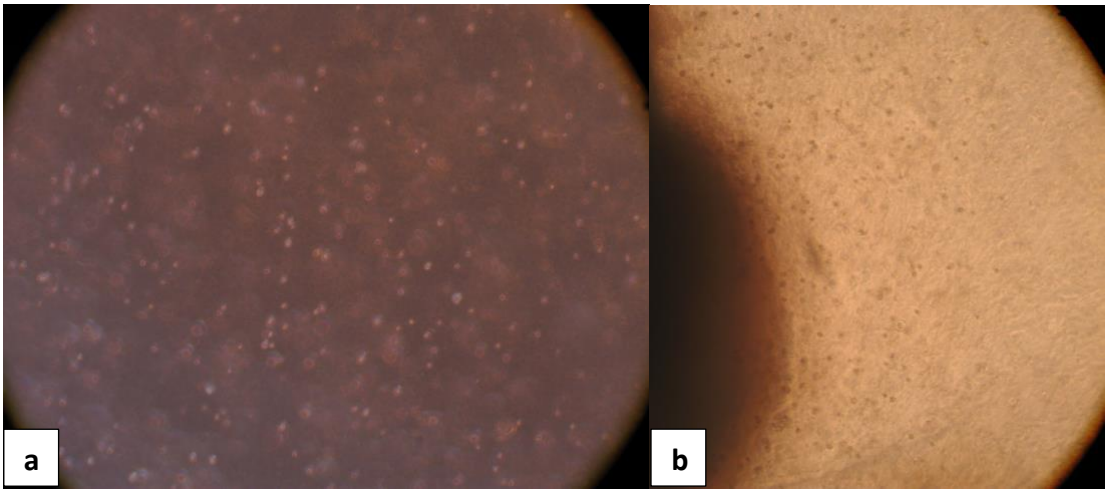

Figure 9. a) 3D model with no nanobeads seen under the microscope showing cells within the gel matrix. b) 3D model with nanobeads in the center of the model. Nanobeads can be seen on the left of the image with the cells surrounding it.

3.4 RESULTS

3.4.1 Proliferation Assay

Proliferation of prostate cancer cell lines; LAPC4 and 22RV1 in comparison to osteoblasts were performed with the cells in different environments; Vehicle (PBS1x) and Zoledronate with the following concentrations in µM; 10, 50 and 100. Figure 10a presents proliferation result of LAPC4 over 24 hours showing significantly reduced proliferation with Zoledronate concentration of 10 and 100 µM (0.471 ± 0.228, p value = 0.0159 and 0.711 ± 0.180 p value = 0.0497) respectively.

Similarly, Figure 10b shows proliferation of LAPC4 over 48 hours with the same conditions as seen in Figure 10. There is no statistical significance between any of the variables and the control, PBS1x.

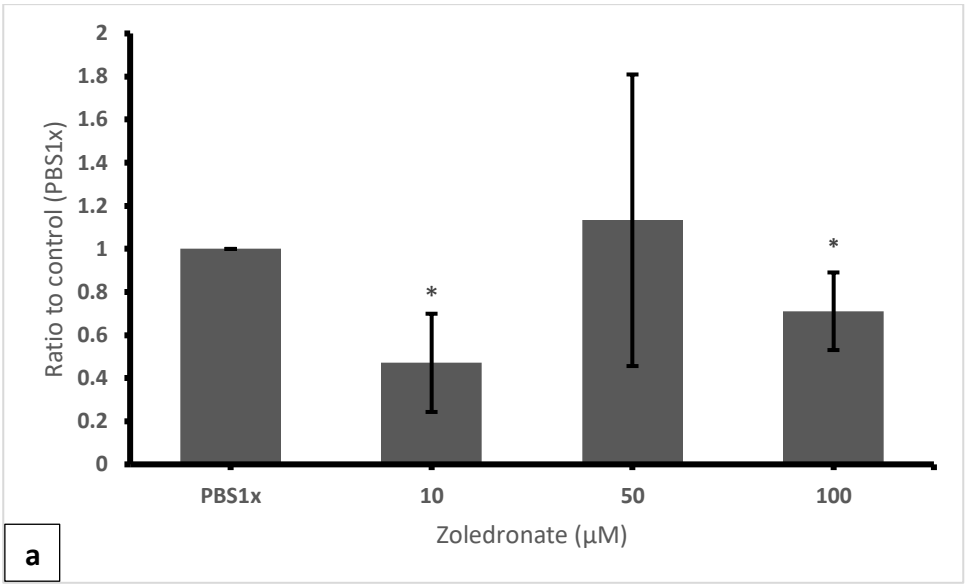

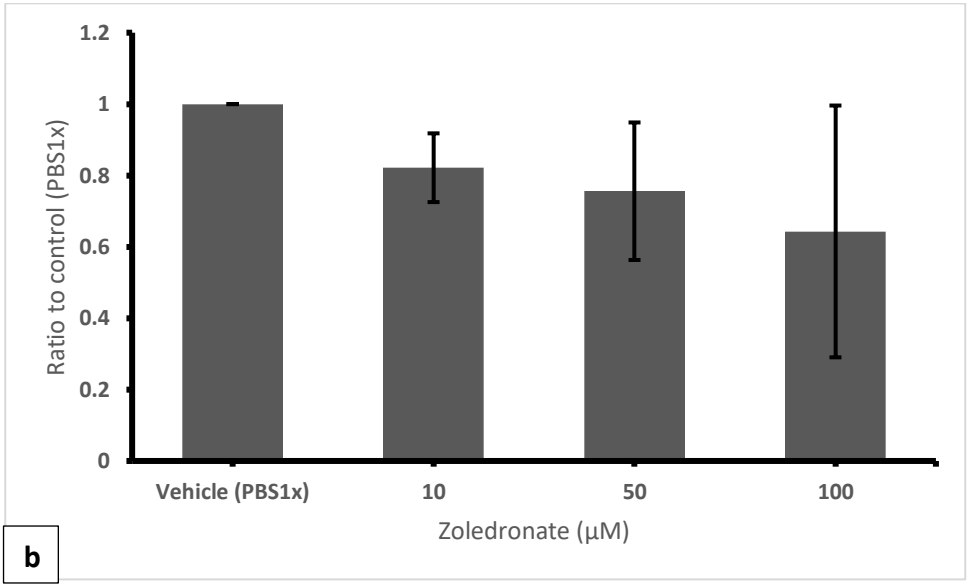

*Figures 10 a-b. Proliferation results using MTT assay for LAPC4 over 24 (Fig 10a) and 48 hours (Fig. 10b) with the following variables; PBS1x, Zoledronate 10, 50, 100 µM. * represents $p < 0.05$.*

Figure 11 present 22RV1 cell proliferation result over 24 (Fig. 11a) and 48 hours (Fig. 11b) hours. No statistical significance was found between the different variables; *Zoledronate 10, 50, 100 µM* and the control, PBS1x for both 24 and 48 hours of culture.

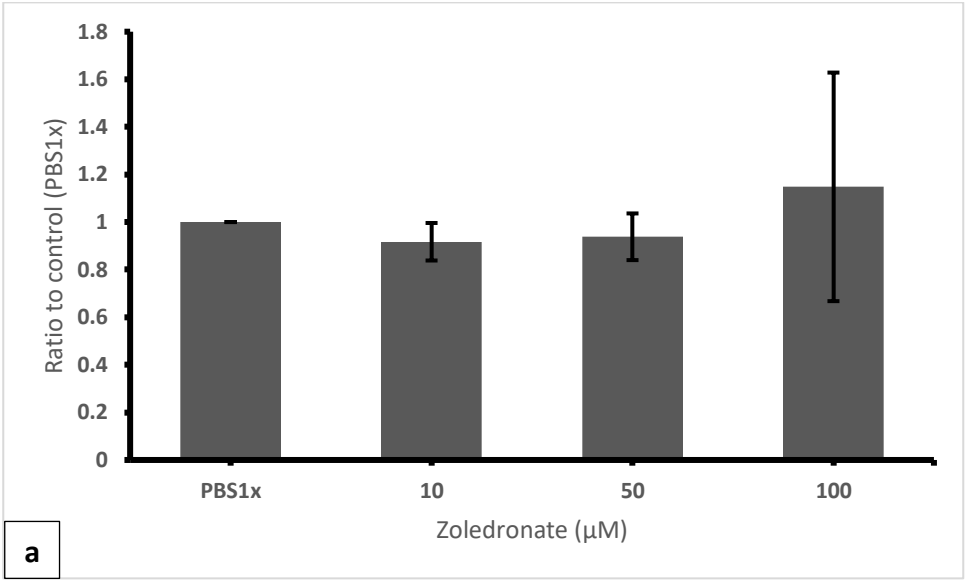

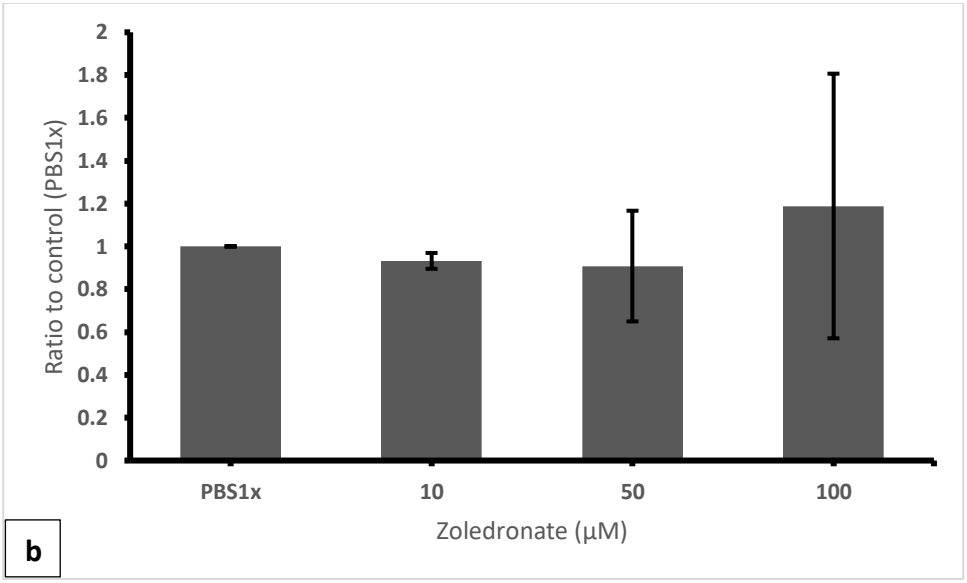

*Figures 11a-b. Proliferation results using MTT assay for 22RV1 over 24 (Fig. 11a) and 48 hours (Fig. 11b) with the following variables; PBS1x, Zoledronate 10, 50, 100 µM. * represents p < 0.05.*

Figure 12 shows proliferation of osteoblast cells in different variables. The highest concentration of Zoledronic acid (100 µM) was found to significantly reduce proliferation of the osteoblast cells (0.698 ± 0.0.52, p value = 0.0145). No significant difference was found with any of the lower concentrations of Zoledronate.

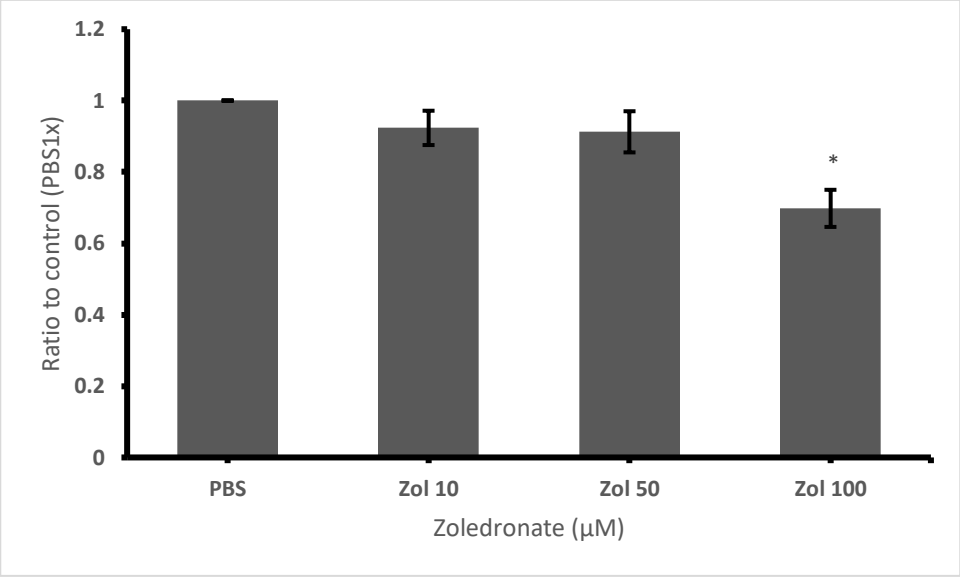

*Figure 12. Bar chart presenting proliferation results using MTT assay for Osteoblasts over 24 hours for the following variables; PBS1x, Zoledronate 10, 50, 100 µM. * represents p < 0.05.*

Figure 13 shows proliferation of PC3 prostate cancer cells with different Zoledronic acid concentrations. Results show that the highest concentration of Zoledronic acid (100 µM) was found to significantly reduce proliferation of the PC3 cells (0.575 ± 0.212, p=0.02571).

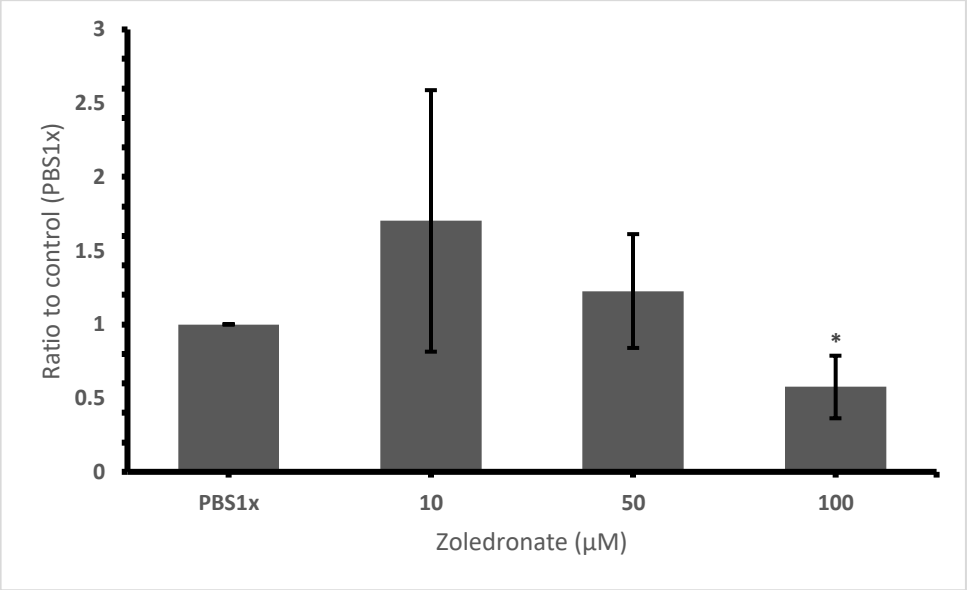

*Figure 13. Proliferation results using MTT assay for PC3 cells over 24 hours for the following variables; PBS1x, Zolendronate 10, 50, 100 µM. * represents p < 0.05.*

3.4.2 Migration Assay

Migration study using the Boyden chamber technique was performed to check migration of LAPC4. Compared to the vehicle control, it was found that LAPC4 cell migration was significantly decreased following treatment with 10 µM Zoledronate (22.8% ± 8.1, p value = 0.04) following 1-week of treatment (Fig. 14)

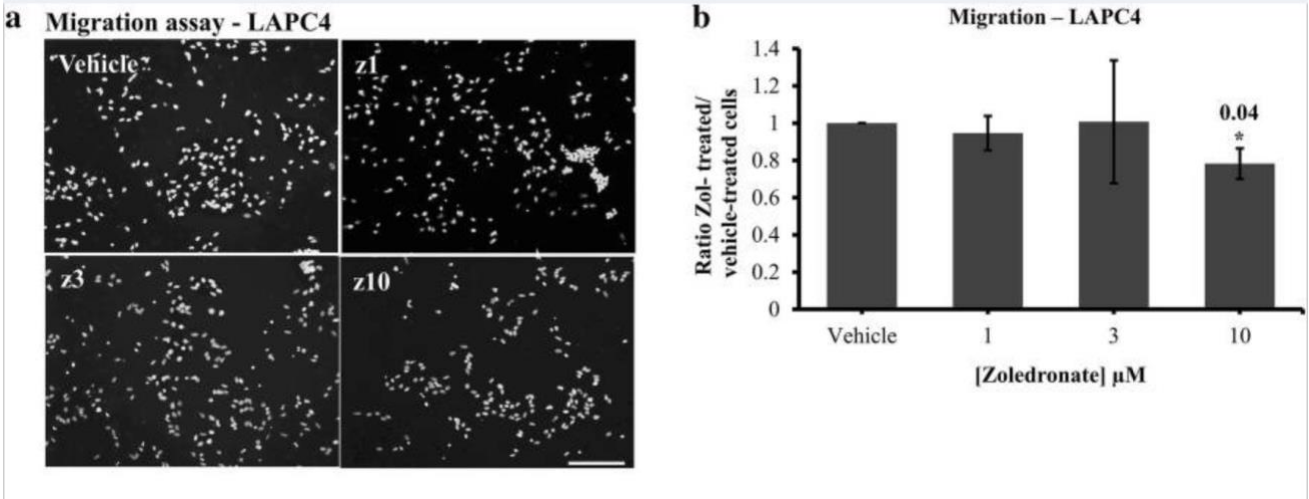

Figure 14. Migration of LAPC4 treated with vehicle (PBS1x) or Zoledronate 1 µM, 3 µM and 10 µM for 7 days in 1% serum condition, a) shows LAPC4 cells and b) represents ratio of drug-treated cells divided by vehicle-treated cells for LAPC4.

3.4.3 Live Dead Viability / Cytotoxicity Assay

To examine cell activity in regard to Zoledronic acid treatment, my group have previously conducted Live/Dead® assay which showed that treatment with 1, 3 and 10 µM Zoledronate did not alter the percent-viable cells, however the total number of cells did in fact reduce significantly with doses higher than 10 µM Zoledronate treatment (live cells 41.1% ± 29.7%, p value = 0.01, dead cells 46.1% ± 14.7%, p value = 0.002) (Fig. 15).

7-day treatment with 100 µM showed significant decrease in percent viable cells (59.1% ± 16.8% p value = 0.03) and the total number of live and dead cells (live cells 89.5% ± 1.82%, p value < 0.001, dead cells 81.4% ± 13.7.7%, p value < 0.001) (Fig. 17). It was interestingly seen that at 14-days with

treatment, cell viability was similar to the 7-day treatment with the difference that that 100 µM of Zoledronate led to near complete cell death.

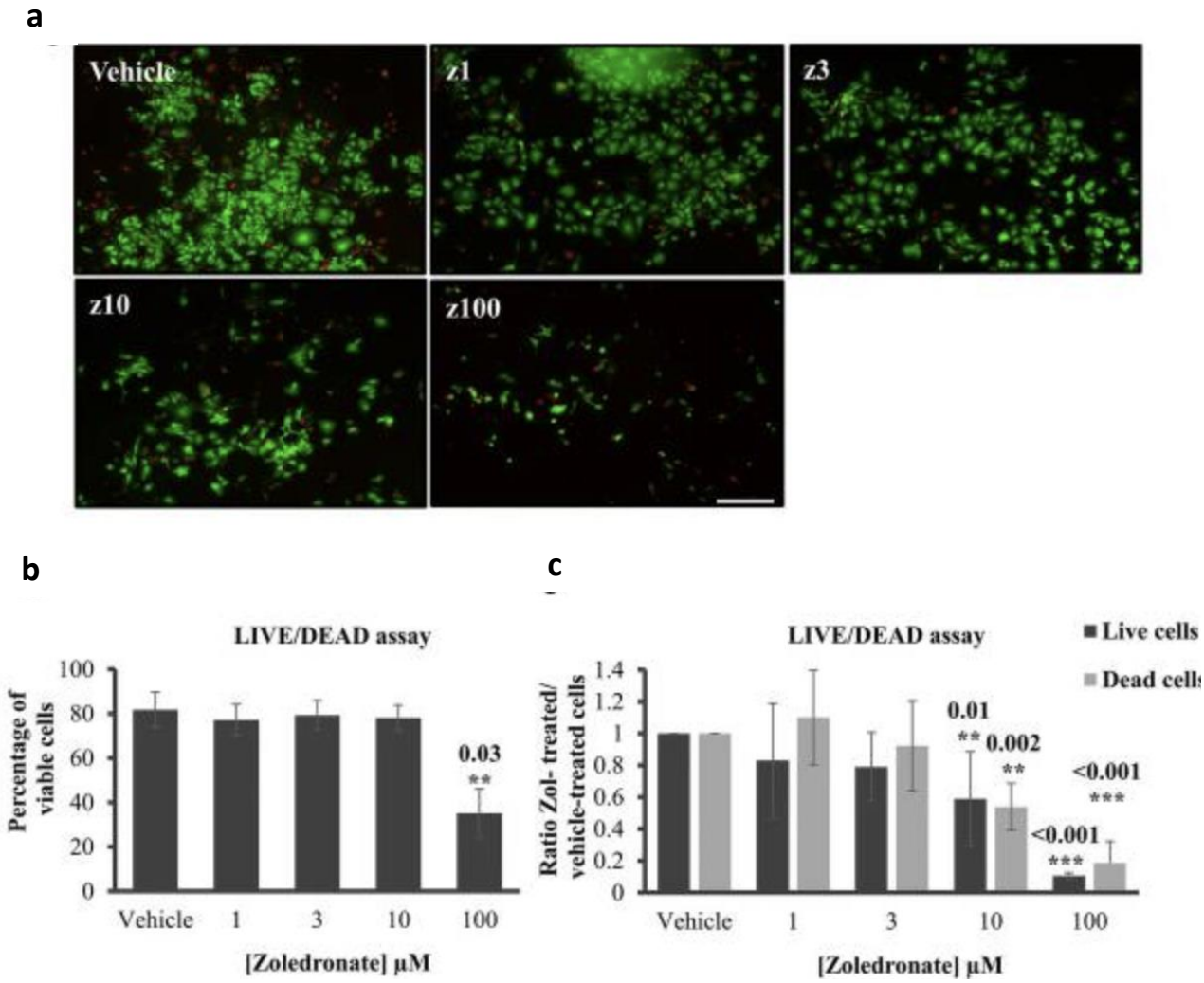

*Figure 15. Representative photos of Live/Dead assay performed for LAPC4 following vehicle or Zoledronate treatment with the following concentrations; 1, 3, 10, 100 µM. a) Live cells are in green and dead cells are in red. b) Percentage of viable cells [number of live cells/(number of live cells + number of dead cells) * 100] and c) ratio of live cells or dead cells in vehicle or Zoledronate treated conditions. Results are mean ± SD, $p < 0.05$. Modified from work done by my previous group (Akoury et al., 2019).*

3.4.4 Scratch Assay

Scratch assays were performed to check migration of PC3 cell lines (Fig. 18). Compared to vehicle (PBS1x), it was found that PC3 cell migration was significantly decreased following treatment with Zoledronate 100 µM at both 18 hours and subsequently at 24 hours (ratio 0.443 ± 0.024, p value = 0.047 and 0.375 ± 0.003, p value = 0.002) as shown in Figure 16.

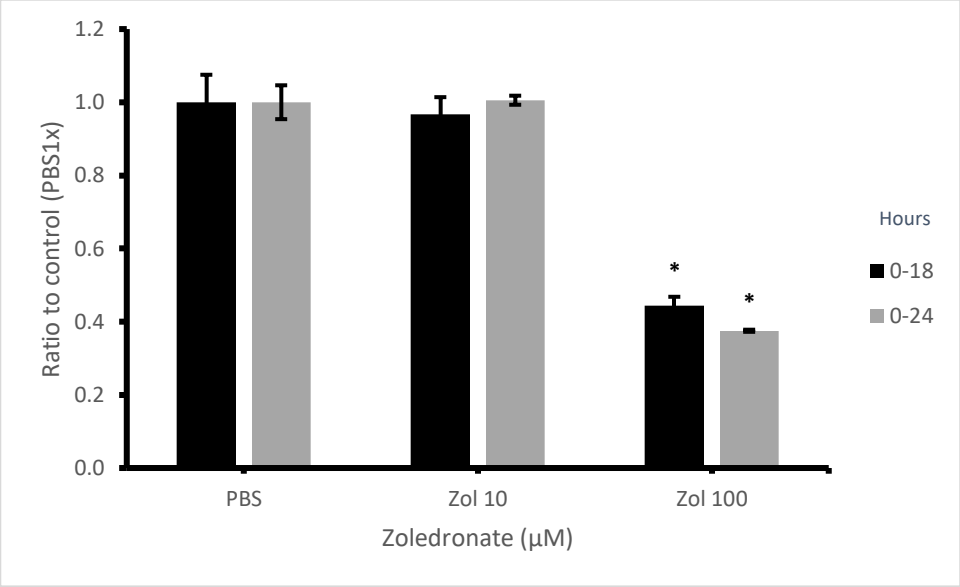

*Figure 16. Migration results using a scratch assay for PC3 cells over 18 and 24 hours for the following variables; PBS1x, Zoledronate 10 and 100 µM. * represents p < 0.05.*

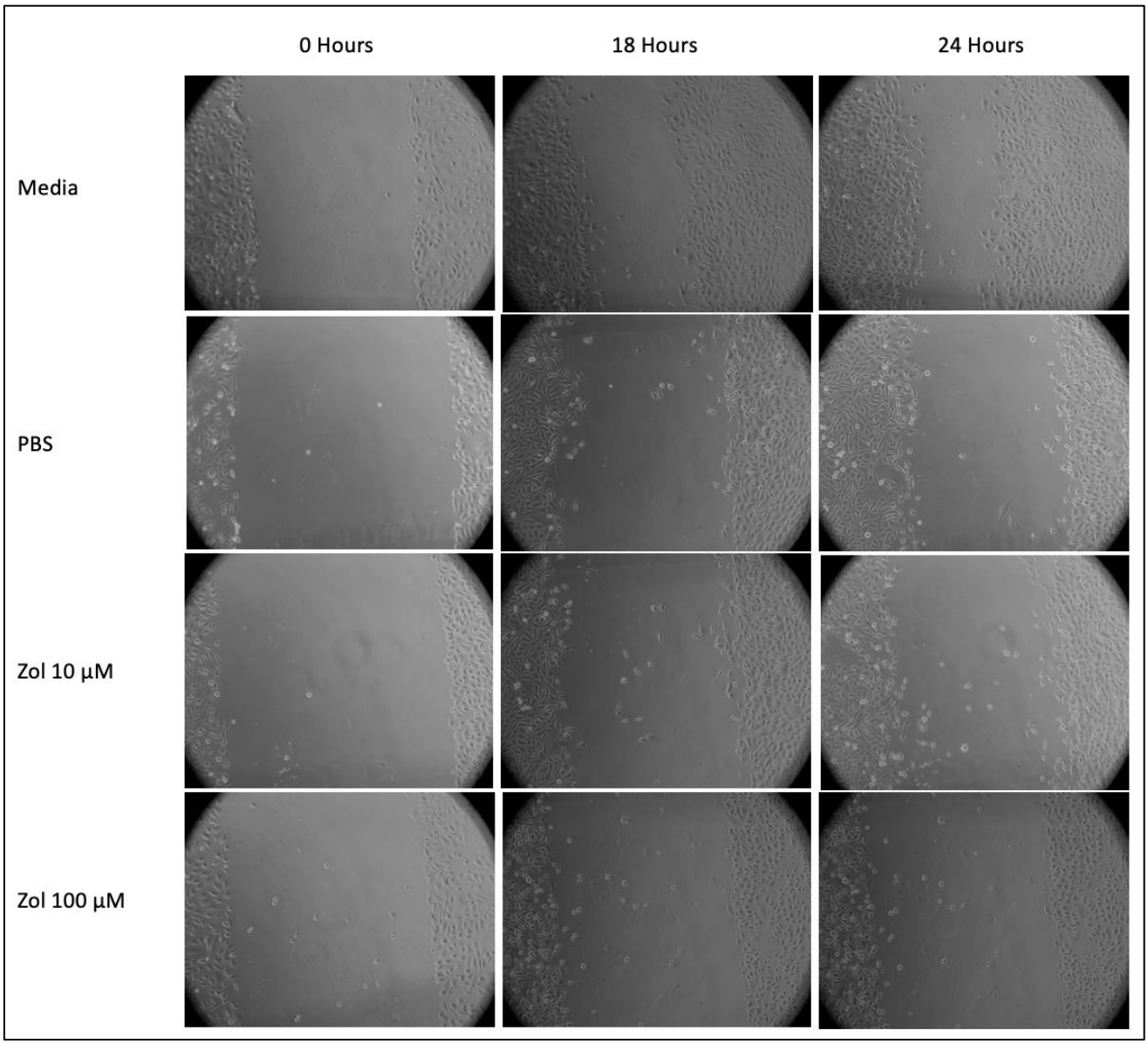

Figure 17. Scratch assay analysis of PC3 cancer cell line at 0, 18 and 24 hours (columns) with different variables; control, vehicle (PBS1x), Zoledronate 10 µM and Zoledronate 100 µM (rows).

3.4.5 3D Osteoblast Model

3D osteoblast model was produced using human bone-marrow derived stem cells to show the capacity of converting stem cells to osteoblasts using osteogenic media and it was used to test a 3D model capacity for further experiments. Figure 18 shows images taken using a microscope of each variable, comparing the models placed in DMEM vs Osteogenic media.

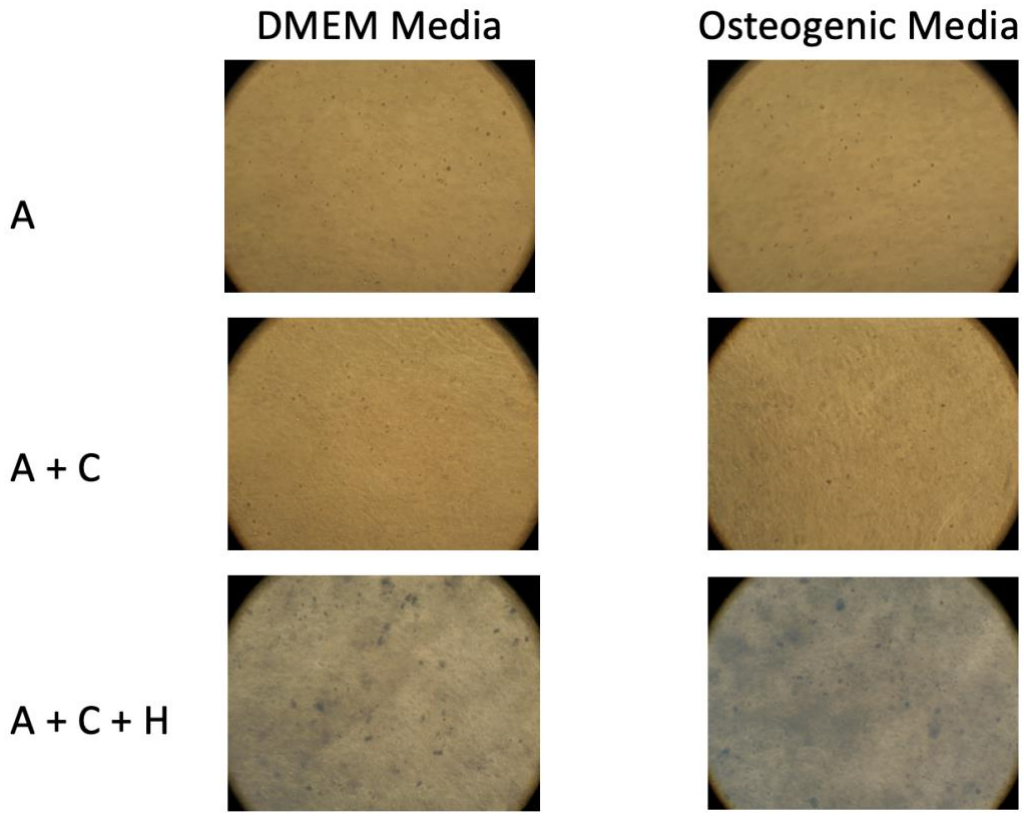

Figure 19.

Fig 18. Images taken using a microscope of each 3D model taken with different variables: A – Agarose, C – Collagen, H – Hydroxyapatite. Images in left column represent models in DMEM media and right column represents models in osteogenic media showing osteoblast formation.

3.4.6 Nanobead preparation

Initially the nanobeads were prepared using fluorescently labeled Zoledronic acid (Fam-Zol) to check binding ability with the nanobeads. Figure 19 shows the increased binding capacity of nanobeads for Fam-Zol when coated with chitosan.

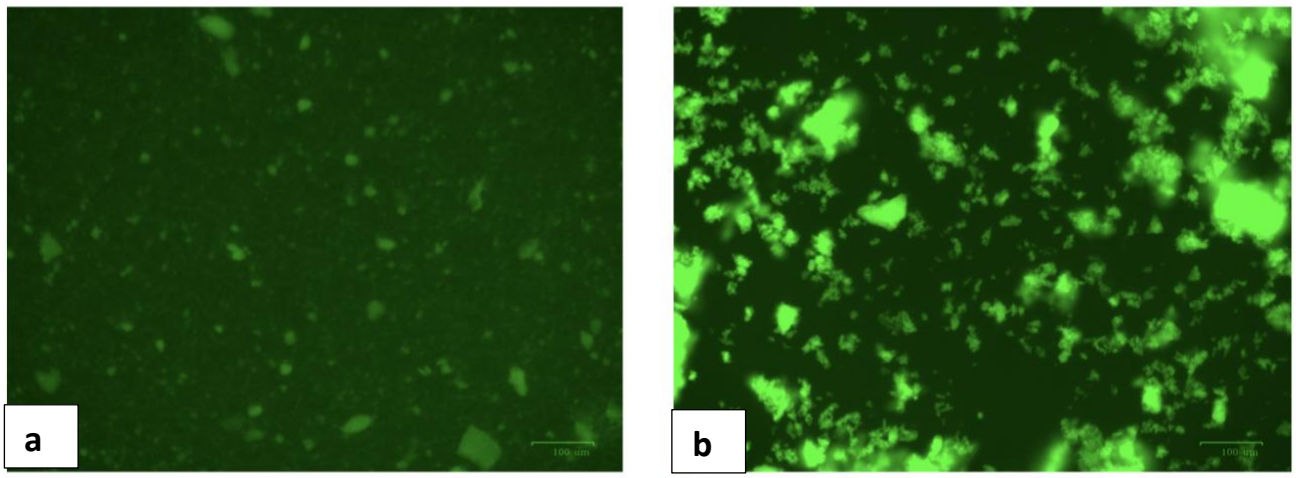

Figure 19. Images from ZOE microscope showing fluorescence activity of nanobeads without chitosan coating (a) and nanobeads coated with chitosan (b).

3.4.7 Nanobead Fam-Zol Experiments

Experiments analyzing nanobead Fam-Zol interaction was done through 3 different experiments. First experiments looked at nanobead release of Fam-Zol over 14 days. As shown in Figure 20, it is important to note the difference between carrying capacity of the nanobeads with and without chitosan. Chitosan coated nanobeads held 48.204 ± 6.195 µl (p value = 0.00076) more than the non chitosan coated nanobeads on day 1. When looking at release of Fam-Zol per 24 hours there is statistical significance between Day 1 and each of the days up until day 7 with chitosan.

Subsequently when focussing on the chitosan coated nanobeads, it can be seen there is a large release of Fam-Zol on day 1 and 2 of 78.65 ± 7.77 and 73.16 ± 17.80 µl respectively. Figure 21 shows the cumulative release of Fam-Zol from the chitosan coated nanobeads and it is clear that there is a steady release of Fam-Zol for 8 days which then starts to level off after this.

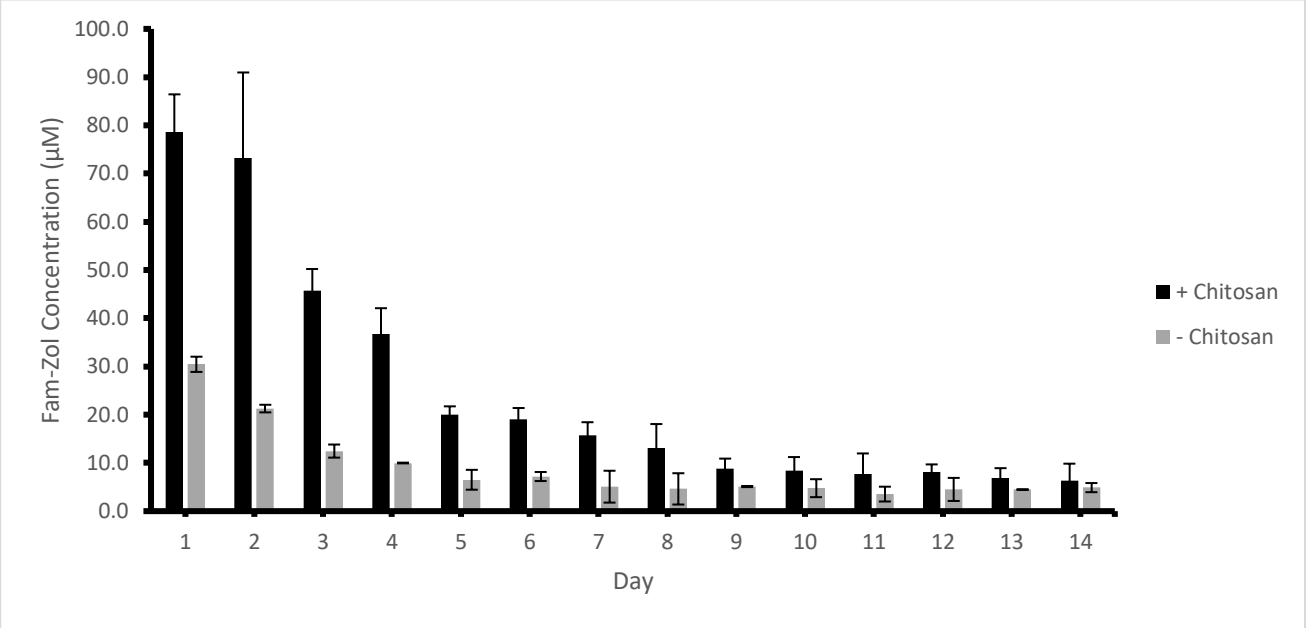

Figure 20 Release of Fam Zol from nanobeads in µl per 24 hours for a total of 14 days (Black bars = Nanobeads coated in chitosan, Grey bars = no chitosan coated nanobeads).

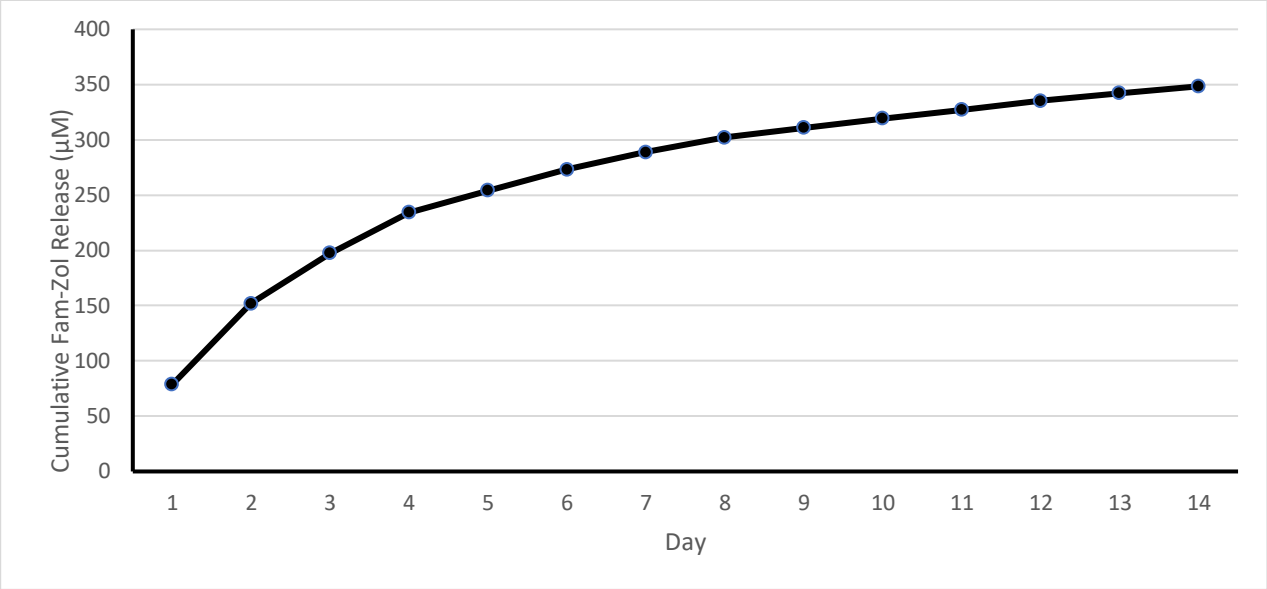

Figure 21. Cumulative release of Fam-Zol from nanobeads in µl per 24 hours for a total of 14 days.

Experiments were also conducted looking at the release of Fam-Zol from bone putty which was mixed with Fam-Zol coated nanobeads. As Figure 22 shows, there is no significant difference in the amount of Fam-Zol released every 24 hours and no difference was found between the chitosan coated Vs no chitosan coated nanobeads over 10 days. No difference was found between the chitosan coated or no chitosan coated nanobeads.

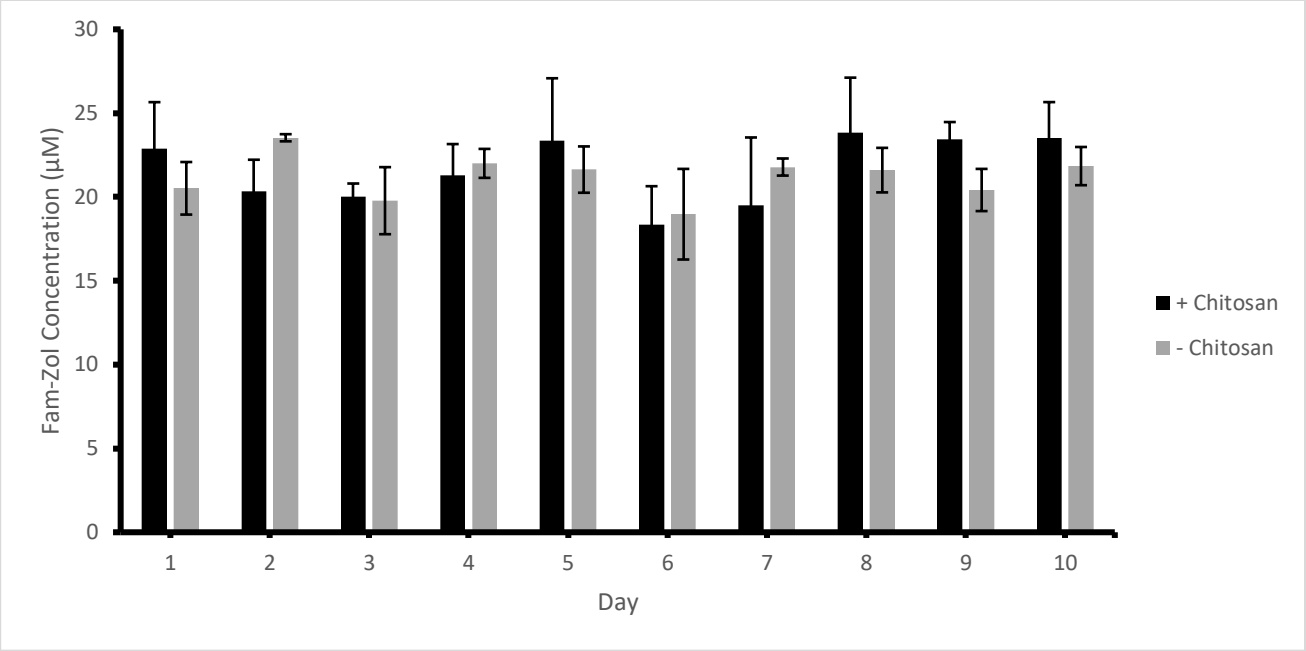

Figure 22. Release of Fam-Zol from nanobeads mixed in with bone putty per 24 hours for a total of 10 days (Black bars = Nanobeads coated in chitosan, Grey bars = no chitosan coated nanobeads).

Next, in terms of Nanobead experiments, experiments were conducted looking at the absorption of Fam-Zol to bone putty from nanobeads dispersed in PBS above the bone construct. As can be seen in Figure 23 there is statistically significant difference in the amount of Fam-Zol still present in PBS between day 1 and 2 (difference of 57.552 ±5.365, p value = 0.0008) in the chitosan coated nanobeads. Similarly, for the non chitosan coated nanobeads a significant difference was seen between day 1 and 2 (difference of 10.847 ± 1.941, p value = 0.004). After Day 2 there is no significant difference between the amount of Fam-Zol still present in the PBS each 24 hours for a total of 10 days, in both the coated and non-coated nanobeads.

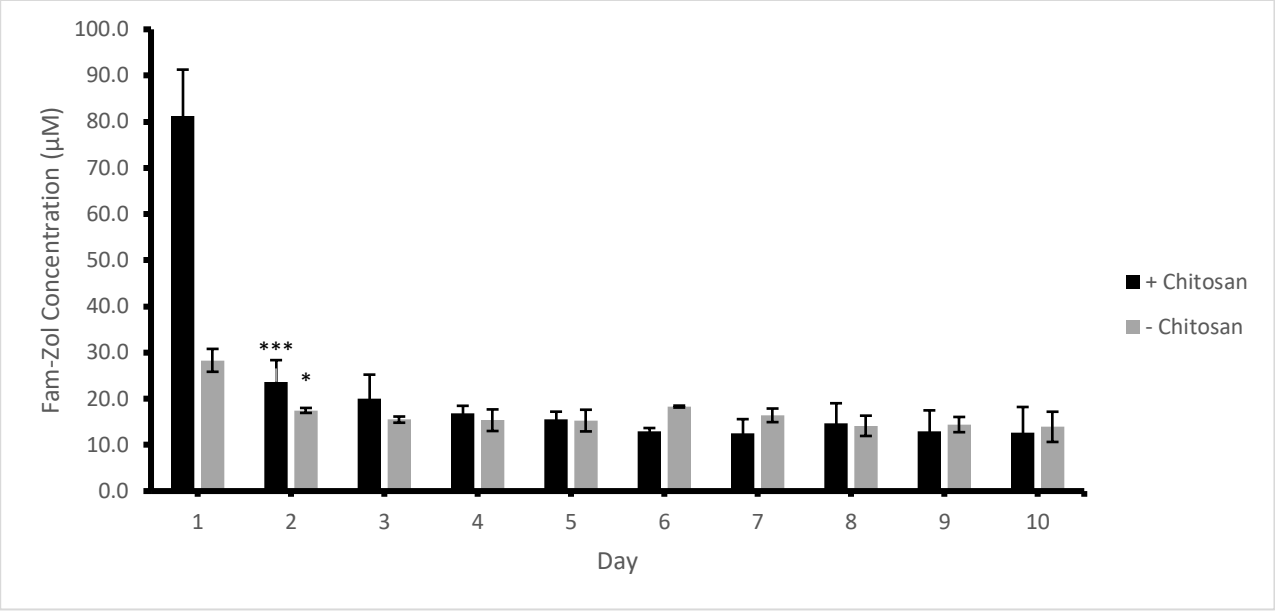

*Figure 23. Absorption of Fam-Zol from nanobeads in PBS sitting above bone putty per 24 hours for a total of 10 days (Black bars = Nanobeads coated in chitosan, Grey bars = no chitosan coated nanobeads). It is a proxy to show the absorption capacity of the bone putty of the Fam Zol. * represents $p < 0.05$, ** represents $p < 0.01$, *** represents $p < 0.001$.*

Finally, we looked at the 3D bioprinted model and their activity on C42B prostate cancer cell lines. As can be seen on Figure 24, initially we looked at the direct effect of Zoledronate on the 3D bioprinted construct and we found a statistically significant reduction in proliferation in the highest dose tested of x100 Zoledronate (x1 = 290.1ng) (ratio 0.6172 ± 0.178, p value = 0.02). We also found an increased statistically significant difference with x5 Zoledronate (ratio 1.355 ± 0.178, p value = 0.0258).

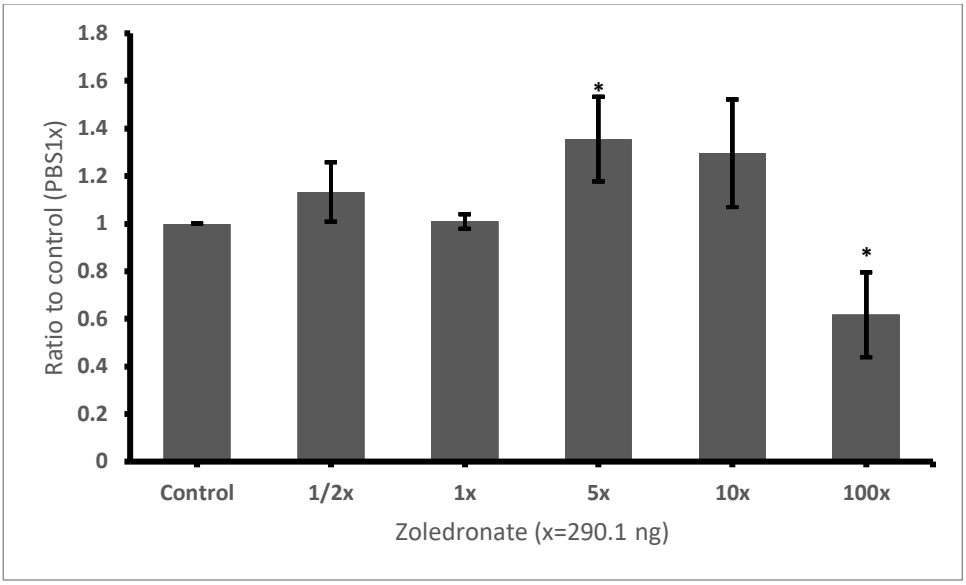

*Figure 24. Ratio difference in the 3D model (C42B cell line) with direct treatment of the different variables; control (PBS1x, 1/2x, 1x, 5x, 10x, 100x Zoledronate (290.1 ng) doses. * represents $p < 0.05$*

Following this we evaluated the proliferation of the C42B cancer cell line when treated with the Zoledronate loaded nanobeads as can be seen on Figure 25. We found statistical significant difference with the 1/2x Zoledronate (x1 = 290.1ng) (ratio 1.511 ± 0.246, p value = 0.023). No other variable showed statistical significance, but it can be seen that with the high dose there appears to be a trend going towards a significant reduction in proliferation as expected.

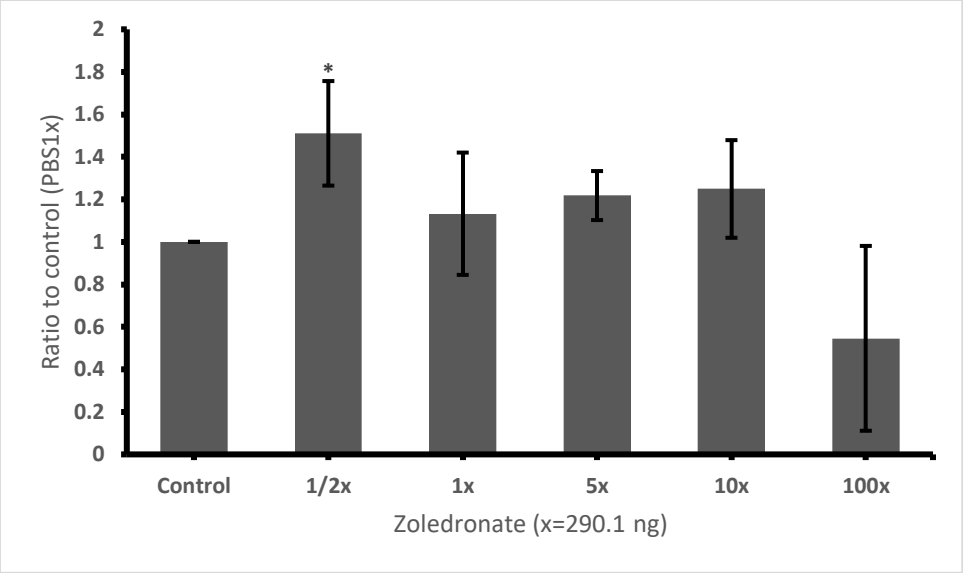

Figure 25. Ratio difference with the 3D model (C42B cell line) with Zoledronate loaded nanobead treatment of the different variables; control (PBS) 1/2x, 1x, 5x, 10x, 100x Zoledronate (290.1 ng) doses.

** represents $p < 0.05$*

Chapter 4 – Discussion and Conclusion

The morbidity and mortality associated with spinal metastases, with up to 40% of all patients with cancer suffering from spinal metastases (Walsh et al., 1997). Patients with spinal metastases endure a large number of complications with the eventual possibility of spinal vertebral fractures or paralysis. Current practice involves a multidisciplinary team and looks at resection of spinal tumors and then supplementing this with chemotherapy and/or radiotherapy depending on the characteristics of the primary cancer (Laufer et al., 2013). This process is extremely difficult for patients and may leave them with even more sequelae due to the systemic administration of the medication, such as pain, nausea and further spinal instability. Studies have shown that patient outcome following this treatment is dependent on the primary tumor characteristics and patient general well-being, with only 10 to 20% being alive after 2 years of diagnosis (Bilsky, Laufer, & Burch, 2009). With the advancements of treatment, the life expectancy of spinal metastasis patients are improving continuously (Falicov et al., 2006). For this reason a huge focus on improving the quality of life of these patients with the main goals being; pain management, stabilization of the spine, maintaining neurological function and controlling the disease at the local level (Rose et al., 2011).

Aspects of spinal metastasis management that our group is interested in involves the local control of tumor and improving stabilization of the spine following tumor resection. Currently, mechanical instability is assessed using the widely known Spinal Instability Neoplastic Score (SINS Score) (Pennington et al., 2019) which looks at different elements of the tumor and predicts the stability and thus guides management decisions. Spinal stabilization is currently obtained using pedicle screw fixation (Joaquim, Powers, Laufer, & Bilsky, 2015) and/or bracing but this does not tackle the issue of

local recurrence and control of the tumor. For this reason, this study looked at ways to load silica nanobeads with Zoledronic acid, a bisphosphonate with anti-tumor effects for the local delivery of this drug to cancer cells.

In this study, the anti-tumor properties of Zoledronic acid were investigated on different prostate cancer cell lines. Proliferation of LAPC4, 22RV1 and PC3 prostate cancer cell lines was investigated for up to 48 hours in Zoledronate doses of 10, 50 and 100 µM. A reduction in proliferation was found in LAPC4 at the highest dose of 100 µM and surprisingly also at 10 µM. Similarly, PC3 proliferation was reduced at the high dose of 100 µM at 24 hours. All other concentrations of Zoledronic acid at 24 or 48 hours for LAPC4, 22RV1 and PC3 cancer cells showed no difference to the control. Additionally, it is important to note that the same experiment was performed on osteoblast cells to check for the safety of the drug, and the highest concentration of 100 µM was found to significantly reduce the proliferation of the cells. These findings match our expectation of the anti-tumor effects on LAPC4 and PC3 cells but further studies with different concentrations and longer treatment durations are required to understand its effects on 22RV1. These results are similar to ones found by Akoury et al. looking at LAPC4 cell proliferation over a week with similar Zoledronic acid doses (Akoury et al., 2019). Additionally, 7 day treatment with doses as high as 100 µM found significant reduction in percent viable cells and the total number of live/dead cells. Our results suggest that high concentrations of Zoledronic acid can be damaging to prostate cancer cells but also healthy osteoblast cells which makes finding the therapeutic dose that can be safe for local control of tumors ever so important.

Cell migration is an important part of metastases as it allows invasion of the tumor cell. We used Falcon™ cell culture inserts to investigate cell migration over 7 days for Zoledronic acid concentrations

of 1, 3 and 10 µM on LAPC4 cells. It was found that cells treated with 10 µM had reduced migration capacity. This suggests that a dose of at least 10 µM is required to impede the migration of LAPC4 cancer cell lines. To assess migration, we also undertook scratch assays of PC3 cancer cell lines. We found a significant reduction in migration with the highest Zoledronic dose used of 100 µM over 18 and 24 hours. These results help us understand the ability of Zoledronic acid to impede prostate cancer cell migration and thus possibly invasion. To make a generalized statement in regard to prostate cancer and migration, more cell lines and Zoledronic acid concentrations will need to be investigated.

As eluded to previously, Zoledronic acid is currently delivered systemically to spinal metastasis patients at high doses of 4 mg dose for 15 min every 3–4 weeks (Di Salvatore et al., 2011). This has side effects ranging from generalized fatigue, renal injury and osteonecrosis of the jaw (Macedo et al., 2017). Additionally, when given systemically, the peak dose only remains in the body for a few hours at 1-3 µM due to the high affinity of bone to Zoledronic acid (Akoury et al., 2019). Our group has previously shown that local delivery of Zoledronic acid using a catheter in a mice model inhibits tumor induced osteolysis and reduces tumor cell proliferation (Nooh et al., 2017). This is not feasible clinically in humans and thus a lot of work is looking at the local delivery of bisphosphonate drugs using carriers such as poly lactide-glycolide acid (PLGA) nanoparticles (Ramanlal Chaudhari et al., 2012), zolendronate loaded hydroxyapatite and calcium phosphate bone cement (Koto et al., 2017) (Sorensen et al., 2013).

With the focus of this study on delivering Zoledronic acid locally we looked to silica nanobeads to act as this drug carrier. Our results show that we have developed a reproducible protocol which enables

us to load nanobeads with Zoledronic acid. The nanobead Fam-Zol release studies prove that the nanobeads are in fact able to contain the drug and release them gradually over the first 8 days of experimentation. Furthermore, we showed that with these nanobeads there was a stable cumulative release of the Fam-Zol showing the potential for localized and steady drug delivery. We found no release of Fam-Zol when it was mixed in with the bone putty and we feel this is the case due to the high affinity of bone to bisphosphonate drugs. Additionally, when we looked at bone absorption into bone putty we found a significant drop in Fam-Zol following day 2 of the experiment suggesting a high volume of the drug bound early on in the experiment to the bone putty due to its high affinity once again.

We combined the findings found from Zoledronic acid action on cancer cell lines and nanobead drug delivery capacity to create a 3D in-vitro model. Using a bioprinter we formed 3D discs seeded with the prostate cancer cell line, C42B. Following this, we placed the Zoledronate coated nanobeads in the middle of this disc to emulate the placement of such a construct in a bone void formed after spinal metastasis resection. In the 3D models which had the Zoledronate loaded nanobeads, we found a general trend showing reduced proliferation of the prostate cancer cell line with higher concentrations of Zoledronic acid suggesting that in an *in-vitro* model we are able to target prostate cancer cells using nanobeads as our drug delivery tool. However, this was not a statistically significant reduction which might be due to different limitations. The 3D model construct might in fact make it difficult for the drug to actually penetrate the gel and interact with the cancer cells. In addition to this, conducting the same experiment with different prostate cancer cell lines and higher number of experiments will enable us to form a more firm conclusion. In comparison, we conducted a 3D model

with direct delivery of the Zoledronate drug which did show a statistically significant reduction in proliferation with the highest dose of Zoledronate (x100) (ratio 0.6172 ± 0.178, p value = 0.02) as expected.

Conclusion

In this study we investigated a potential future direction of local management of prostate cancer cell spinal metastasis. We started by showing the anti-tumor effects of Zoledronate on various prostate cancer cell lines and how with relatively low doses this can be achieved. Subsequently our work with silica nanobeads proved we are able to successfully coat these with a therapeutic Zoledronic acid dose. In our 3D *in-vitro* model, we were able to show the local delivery of Zoledronic acid and its anti-tumor effect on a prostate cancer cell line. Current practice of systemic administration of bisphosphate drugs in spinal metastasis patients leads to substantial side effects such as generalized fatigue, gastrointestinal symptoms and osteonecrosis of the jaw (Umunakwe et al., 2017). Our study shows that we are able to deliver a bisphosphonate drug, Zoledronic acid, safely, inexpensively and at therapeutic levels locally using nanobead technology.

Our future vision for this work involves mice models with integrated spine metastasis. Our goal is to deliver Zoledronic acid locally following tumor resection to reduce its systemic side effects whilst still reaching anti-tumor effects. Additionally, we wish to devise a more structurally stable method to deliver the drug coated nanobeads such as within bone cement to provide structural strength and the local delivery of the drug following tumor resection. Finally, we wish to explore the effect of

Zoledronic acid action on other cancer cell types with high spinal metastasis risk such as breast and lung cancer to determine the effect of this method of drug delivery in other settings.

Chapter 5 – Bibliography

Aebi, M. (2003). Spinal metastasis in the elderly. *European Spine Journal, 12 Suppl 2*, S202-213. doi:10.1007/s00586-003-0609-9

Ahangar, P., Aziz, M., Rosenzweig, D. H., & Weber, M. H. (2019). Advances in personalized treatment of metastatic spine disease. *Ann Transl Med, 7*(10), 223. doi:10.21037/atm.2019.04.41

Akoury, E., Ahangar, P., Nour, A., Lapointe, J., Guerard, K. P., Haglund, L., . . . Weber, M. H. (2019). Low-dose zoledronate for the treatment of bone metastasis secondary to prostate cancer. *Cancer Cell Int, 19*, 28. doi:10.1186/s12935-019-0745-x

Almubarak, H., Jones, A., Chaisuparat, R., Zhang, M., Meiller, T. F., & Scheper, M. A. (2011). Zoledronic acid directly suppresses cell proliferation and induces apoptosis in highly tumorigenic prostate and breast cancers. *J Carcinog, 10*, 2. doi:10.4103/1477-3163.75723

Bartanusz, V., & Porchet, F. (2003). Current strategies in the management of spinal metastatic disease. *Swiss Surg, 9*(2), 55-62. doi:10.1024/1023-9332.9.2.55

Bilsky, M. H., Laufer, I., & Burch, S. (2009). Shifting paradigms in the treatment of metastatic spine disease. *Spine (Phila Pa 1976), 34*(22 Suppl), S101-107. doi:10.1097/BRS.0b013e3181bac4b2

Black, D. M., Delmas, P. D., Eastell, R., Reid, I. R., Boonen, S., Cauley, J. A., . . . Trial, H. P. F. (2007). Once-yearly zoledronic acid for treatment of postmenopausal osteoporosis. *N Engl J Med, 356*(18), 1809-1822. doi:10.1056/NEJMoa067312

Bobyn, J. D., McKenzie, K., Karabasz, D., Krygier, J. J., & Tanzer, M. (2009). Locally delivered bisphosphonate for enhancement of bone formation and implant fixation. *Journal of Bone & Joint Surgery - American Volume, 91 Suppl 6*, 23-31. doi:10.2106/JBJS.I.00518

Croucher, P. I., McDonald, M. M., & Martin, T. J. (2016). Bone metastasis: the importance of the neighbourhood. *Nat Rev Cancer, 16*(6), 373-386. doi:10.1038/nrc.2016.44

Cui, X., & Boland, T. (2009). Human microvasculature fabrication using thermal inkjet printing technology. *Biomaterials, 30*(31), 6221-6227. doi:10.1016/j.biomaterials.2009.07.056

Czarnobaj, K. (2008). Preparation and characterization of silica xerogels as carriers for drugs. *Drug Deliv, 15*(8), 485-492. doi:10.1080/10717540802321495

Davarski, A. N., Kitov, B. D., Zhelyazkov, C. B., Raykov, S. D., Kehayov, II, Koev, I. G., & Kalnev, B. M. (2013). Surgical management of metastatic tumors of the cervical spine. *Folia Med (Plovdiv), 55*(3-4), 39-45. doi:10.2478/folmed-2013-0026

Di Pasqua, A. J., Wallner, S., Kerwood, D. J., & Dabrowiak, J. C. (2009). Adsorption of the Pt(II) anticancer drug carboplatin by mesoporous silica. *Chem Biodivers, 6*(9), 1343-1349. doi:10.1002/cbdv.200900021

Di Salvatore, M., Orlandi, A., Bagala, C., Quirino, M., Cassano, A., Astone, A., & Barone, C. (2011). Anti-tumour and anti-angiogenetic effects of zoledronic acid on human non-small-cell lung cancer cell line. *Cell Prolif, 44*(2), 139-146. doi:10.1111/j.1365-2184.2011.00745.x

Drake, M. T., Clarke, B. L., & Khosla, S. (2008). Bisphosphonates: mechanism of action and role in clinical practice. *Mayo Clin Proc, 83*(9), 1032-1045. doi:10.4065/83.9.1032

Falicov, A., Fisher, C. G., Sparkes, J., Boyd, M. C., Wing, P. C., & Dvorak, M. F. (2006). Impact of surgical intervention on quality of life in patients with spinal metastases. *Spine (Phila Pa 1976), 31*(24), 2849-2856. doi:10.1097/01.brs.0000245838.37817.40

Fleisch, H. (1998). Bisphosphonates: mechanisms of action. *Endocr Rev, 19*(1), 80-100. doi:10.1210/edrv.19.1.0325

Gandaglia, G., Karakiewicz, P. I., Briganti, A., Passoni, N. M., Schiffmann, J., Trudeau, V., . . . Sun, M. (2015). Impact of the Site of Metastases on Survival in Patients with Metastatic Prostate Cancer. *Eur Urol, 68*(2), 325-334. doi:10.1016/j.eururo.2014.07.020

Gao, G., Hubbell, K., Schilling, A. F., Dai, G., & Cui, X. (2017). Bioprinting Cartilage Tissue from Mesenchymal Stem Cells and PEG Hydrogel. *Methods Mol Biol, 1612*, 391-398. doi:10.1007/978-1-4939-7021-6_28

Ghidini, T. (2018). Regenerative medicine and 3D bioprinting for human space exploration and planet colonisation. *J Thorac Dis, 10*(Suppl 20), S2363-S2375. doi:10.21037/jtd.2018.03.19

Greenlee, R. T., Murray, T., Bolden, S., & Wingo, P. A. (2000). Cancer statistics, 2000. *CA Cancer J Clin, 50*(1), 7-33. doi:10.3322/canjclin.50.1.7

Gungor-Ozkerim, P. S., Inci, I., Zhang, Y. S., Khademhosseini, A., & Dokmeci, M. R. (2018). Bioinks for 3D bioprinting: an overview. *Biomater Sci, 6*(5), 915-946. doi:10.1039/c7bm00765e

Hsiao, C. P., Daly, B., & Saligan, L. N. (2016). The Etiology and management of radiotherapy-induced fatigue. *Expert Rev Qual Life Cancer Care, 1*(4), 323-328. doi:10.1080/23809000.2016.1191948

Humzah, M. D., & Soames, R. W. (1988). Human intervertebral disc: structure and function. *Anat Rec, 220*(4), 337-356. doi:10.1002/ar.1092200402

Ibrahim, A., Scher, N., Williams, G., Sridhara, R., Li, N., Chen, G., . . . Pazdur, R. (2003). Approval summary for zoledronic acid for treatment of multiple myeloma and cancer bone metastases. *Clin Cancer Res, 9*(7), 2394-2399. Retrieved from https://www.ncbi.nlm.nih.gov/pubmed/12855610

Jereczek-Fossa, B. A., Marsiglia, H. R., & Orecchia, R. (2001). Radiotherapy-related fatigue: how to assess and how to treat the symptom. A commentary. *Tumori, 87*(3), 147-151. Retrieved from https://www.ncbi.nlm.nih.gov/pubmed/11504369

Jereczek-Fossa, B. A., Marsiglia, H. R., & Orecchia, R. (2002). Radiotherapy-related fatigue. *Crit Rev Oncol Hematol, 41*(3), 317-325. doi:10.1016/s1040-8428(01)00143-3

Joaquim, A. F., Powers, A., Laufer, I., & Bilsky, M. H. (2015). An update in the management of spinal metastases. *Arq Neuropsiquiatr, 73*(9), 795-802. doi:10.1590/0004-282X20150099

Joly, F., Ahmed-Lecheheb, D., Thiery-Vuillemin, A., Orillard, E., & Coquan, E. (2019). [Side effects of chemotherapy for testicular cancers and post-cancer follow-up]. *Bull Cancer, 106*(9), 805-811. doi:10.1016/j.bulcan.2019.04.004

Kibler, W. B., Press, J., & Sciascia, A. (2006). The role of core stability in athletic function. *Sports Med, 36*(3), 189-198. doi:10.2165/00007256-200636030-00001

Kim, J. H., Seol, Y. J., Ko, I. K., Kang, H. W., Lee, Y. K., Yoo, J. J., . . . Lee, S. J. (2018). 3D Bioprinted Human Skeletal Muscle Constructs for Muscle Function Restoration. *Sci Rep, 8*(1), 12307. doi:10.1038/s41598-018-29968-5

Koto, K., Murata, H., Sawai, Y., Ashihara, E., Horii, M., & Kubo, T. (2017). Cytotoxic effects of zoledronic acid-loaded hydroxyapatite and bone cement in malignant tumors. *Oncol Lett, 14*(2), 1648-1656. doi:10.3892/ol.2017.6355

Kubackova, J., Zbytovska, J., & Holas, O. (2019). Nanomaterials for direct and indirect immunomodulation: A review of applications. *Eur J Pharm Sci*, 105139. doi:10.1016/j.ejps.2019.105139

Langley, R. R., & Fidler, I. J. (2011). The seed and soil hypothesis revisited--the role of tumor-stroma interactions in metastasis to different organs. *Int J Cancer, 128*(11), 2527-2535. doi:10.1002/ijc.26031

Laufer, I., Rubin, D. G., Lis, E., Cox, B. W., Stubblefield, M. D., Yamada, Y., & Bilsky, M. H. (2013). The NOMS framework: approach to the treatment of spinal metastatic tumors. *Oncologist, 18*(6), 744-751. doi:10.1634/theoncologist.2012-0293

Li, Z., Su, K., Cheng, B., & Deng, Y. (2010). Organically modified MCM-type material preparation and its usage in controlled amoxicillin delivery. *J Colloid Interface Sci, 342*(2), 607-613. doi:10.1016/j.jcis.2009.10.073

Lin, J. F., Lin, Y. C., Lin, Y. H., Tsai, T. F., Chou, K. Y., Chen, H. E., & Hwang, T. I. (2011). Zoledronic acid induces autophagic cell death in human prostate cancer cells. *Journal of Urology, 185*(4), 1490-1496. doi:10.1016/j.juro.2010.11.045

Lin, Y.-C., Liao, P.-C., Tsai, T.-F., Chou, K.-Y., Chen, H.-E., Lin, J.-F., & Hwang, T. I.-S. (2014). Zoledronic Acid Elicits Proinflammatory Cytokine Profile in Osteolytic Prostate Cancer Cells. *ISRN Pathology, 2014*, 8. doi:10.1155/2014/124746

Lipton, A. (2008). Emerging role of bisphosphonates in the clinic--antitumor activity and prevention of metastasis to bone. *Cancer Treat Rev, 34 Suppl 1*, S25-30. doi:10.1016/j.ctrv.2008.03.008

Luz, M. A., & Aprikian, A. G. (2010). Preventing bone complications in advanced prostate cancer. *Curr Oncol, 17 Suppl 2*, S65-71. doi:10.3747/co.v17i0.722

Maccauro, G., Spinelli, M. S., Mauro, S., Perisano, C., Graci, C., & Rosa, M. A. (2011). Physiopathology of spine metastasis. *Int J Surg Oncol, 2011*, 107969. doi:10.1155/2011/107969

Macedo, F., Ladeira, K., Pinho, F., Saraiva, N., Bonito, N., Pinto, L., & Goncalves, F. (2017). Bone Metastases: An Overview. *Oncol Rev, 11*(1), 321. doi:10.4081/oncol.2017.321

Mathews Griner, L. A., Zhang, X., Guha, R., McKnight, C., Goldlust, I. S., Lal-Nag, M., . . . Ferrer, M. (2016). Large-scale pharmacological profiling of 3D tumor models of cancer cells. *Cell Death Dis, 7*(12), e2492. doi:10.1038/cddis.2016.360

McHugh, K. J., Nguyen, T. D., Linehan, A. R., Yang, D., Behrens, A. M., Rose, S., . . . Jaklenec, A. (2017). Fabrication of fillable microparticles and other complex 3D microstructures. *Science, 357*(6356), 1138-1142. doi:10.1126/science.aaf7447

Miettinen, S. S., Jaatinen, J., Pelttari, A., Lappalainen, R., Monkkonen, J., Venesmaa, P. K., & Kroger, H. P. (2009). Effect of locally administered zoledronic acid on injury-induced intramembranous bone regeneration and osseointegration of a titanium implant in rats. *J Orthop Sci, 14*(4), 431-436. doi:10.1007/s00776-009-1352-9

Nevozhay, D., Kanska, U., Budzynska, R., & Boratynski, J. (2007). [Current status of research on conjugates and related drug delivery systems in the treatment of cancer and other diseases]. *Postepy Hig Med Dosw (Online), 61*, 350-360. Retrieved from https://www.ncbi.nlm.nih.gov/pubmed/17554238

Nogawa, M., Yuasa, T., Kimura, S., Kuroda, J., Segawa, H., Sato, K., . . . Maekawa, T. (2005). Zoledronic acid mediates Ras-independent growth inhibition of prostate cancer cells. *Oncol Res, 15*(1), 1-9. doi:10.3727/096504005775082093

Nooh, A., Zhang, Y. L., Sato, D., Rosenzweig, D. H., Tabaries, S., Siegel, P., . . . Weber, M. H. (2017). Intra-tumor delivery of zoledronate mitigates metastasis-induced osteolysis superior to systemic administration. *J Bone Oncol, 6*, 8-15. doi:10.1016/j.jbo.2017.01.001

Patchell, R. A., Tibbs, P. A., Regine, W. F., Payne, R., Saris, S., Kryscio, R. J., . . . Young, B. (2005). Direct decompressive surgical resection in the treatment of spinal cord compression caused by metastatic cancer: a randomised trial. *Lancet, 366*(9486), 643-648. doi:10.1016/S0140-6736(05)66954-1

Pennington, Z., Ahmed, A. K., Westbroek, E. M., Cottrill, E., Lubelski, D., Goodwin, M. L., & Sciubba, D. M. (2019). SINS Score and Stability: Evaluating the Need for Stabilization Within the Uncertain Category. *World Neurosurgery, 128*, e1034-e1047. doi:10.1016/j.wneu.2019.05.067

Popovici, R. F., Seftel, E. M., Mihai, G. D., Popovici, E., & Voicu, V. A. (2011). Controlled drug delivery system based on ordered mesoporous silica matrices of captopril as angiotensin-converting enzyme inhibitor drug. *J Pharm Sci, 100*(2), 704-714. doi:10.1002/jps.22308

Pourchet, L. J., Thepot, A., Albouy, M., Courtial, E. J., Boher, A., Blum, L. J., & Marquette, C. A. (2017). Human Skin 3D Bioprinting Using Scaffold-Free Approach. *Adv Healthc Mater, 6*(4). doi:10.1002/adhm.201601101

Raj, S., Khurana, S., Choudhari, R., Kumar Kesari, K., Kamal, M. A., Garg, N., . . . Kumar, D. (2019). Specific targeting cancer cells with nanoparticles and drug delivery in cancer therapy. *Semin Cancer Biol*. doi:10.1016/j.semcancer.2019.11.002

Ramanlal Chaudhari, K., Kumar, A., Megraj Khandelwal, V. K., Ukawala, M., Manjappa, A. S., Mishra, A. K., . . . Ramachandra Murthy, R. S. (2012). Bone metastasis targeting: a novel approach to reach bone using Zoledronate anchored PLGA nanoparticle as carrier system loaded with Docetaxel. *J Control Release, 158*(3), 470-478. doi:10.1016/j.jconrel.2011.11.020

Reid, I. R., Brown, J. P., Burckhardt, P., Horowitz, Z., Richardson, P., Trechsel, U., . . . Meunier, P. J. (2002). Intravenous zoledronic acid in postmenopausal women with low bone mineral density. *N Engl J Med, 346*(9), 653-661. doi:10.1056/NEJMoa011807

Reid, I. R., Miller, P., Lyles, K., Fraser, W., Brown, J. P., Saidi, Y., . . . Hosking, D. (2005). Comparison of a single infusion of zoledronic acid with risedronate for Paget's disease. *N Engl J Med, 353*(9), 898-908. doi:10.1056/NEJMoa044241

Reuben, J. S., Dinh, L., Lee, J., Stateson, J., Kamara, H., Xiang, L., & Opperman, L. A. (2011). Bisphosphonates inhibit phosphorylation of signal transducer and activator of transcription 3 and expression of suppressor of cytokine signaling 3: implications for their effects on innate immune function and osteoclastogenesis. *Oral Surg Oral Med Oral Pathol Oral Radiol Endod, 111*(2), 196-204. doi:10.1016/j.tripleo.2010.09.068

Riedl, A., Schlederer, M., Pudelko, K., Stadler, M., Walter, S., Unterleuthner, D., . . . Dolznig, H. (2017). Comparison of cancer cells in 2D vs 3D culture reveals differences in AKT-mTOR-S6K signaling and drug responses. *J Cell Sci, 130*(1), 203-218. doi:10.1242/jcs.188102

Rodan, G. A., & Fleisch, H. A. (1996). Bisphosphonates: mechanisms of action. *J Clin Invest, 97*(12), 2692-2696. doi:10.1172/JCI118722

Rose, P. S., Clarke, M. J., & Dekutoski, M. B. (2011). Minimally invasive treatment of spinal metastases: techniques. *Int J Surg Oncol, 2011*, 494381. doi:10.1155/2011/494381

Russell, R. G., & Rogers, M. J. (1999). Bisphosphonates: from the laboratory to the clinic and back again. *Bone, 25*(1), 97-106. doi:10.1016/s8756-3282(99)00116-7

Saad, F., Gleason, D. M., Murray, R., Tchekmedyian, S., Venner, P., Lacombe, L., . . . Zoledronic Acid Prostate Cancer Study, G. (2002). A randomized, placebo-controlled trial of zoledronic acid in patients with hormone-refractory metastatic prostate carcinoma. *J Natl Cancer Inst, 94*(19), 1458-1468. doi:10.1093/jnci/94.19.1458

Santini, D., Barni, S., Intagliata, S., Falcone, A., Ferrau, F., Galetta, D., . . . Tonini, G. (2015). Natural History of Non-Small-Cell Lung Cancer with Bone Metastases. *Sci Rep, 5*, 18670. doi:10.1038/srep18670

Satalkar, P., Elger, B. S., & Shaw, D. M. (2016). Defining Nano, Nanotechnology and Nanomedicine: Why Should It Matter? *Sci Eng Ethics, 22*(5), 1255-1276. doi:10.1007/s11948-015-9705-6

Schaberg, J., & Gainor, B. J. (1985). A profile of metastatic carcinoma of the spine. *Spine (Phila Pa 1976), 10*(1), 19-20. doi:10.1097/00007632-198501000-00003

Sciubba, D. M., Petteys, R. J., Dekutoski, M. B., Fisher, C. G., Fehlings, M. G., Ondra, S. L., . . . Gokaslan, Z. L. (2010). Diagnosis and management of metastatic spine disease. A review. *Journal of Neurosurgery Spine, 13*(1), 94-108. doi:10.3171/2010.3.SPINE09202

Sebaaly, A., Shedid, D., Boubez, G., Zairi, F., Kanhonou, M., Yuh, S. J., & Wang, Z. (2018). Surgical site infection in spinal metastasis: incidence and risk factors. *Spine J, 18*(8), 1382-1387. doi:10.1016/j.spinee.2018.01.002

Selvaggi, G., & Scagliotti, G. V. (2005). Management of bone metastases in cancer: a review. *Crit Rev Oncol Hematol, 56*(3), 365-378. doi:10.1016/j.critrevonc.2005.03.011

Senaratne, S. G., Pirianov, G., Mansi, J. L., Arnett, T. R., & Colston, K. W. (2000). Bisphosphonates induce apoptosis in human breast cancer cell lines. *Br J Cancer, 82*(8), 1459-1468. doi:10.1054/bjoc.1999.1131

Sorensen, T. C., Arnoldi, J., Procter, P., Beimel, C., Jonsson, A., Lenneras, M., . . . Steckel, H. (2013). Locally enhanced early bone formation of zoledronic acid incorporated into a bone cement plug in vivo. *J Pharm Pharmacol, 65*(2), 201-212. doi:10.1111/j.2042-7158.2012.01588.x

Spratt, D. E., Beeler, W. H., de Moraes, F. Y., Rhines, L. D., Gemmete, J. J., Chaudhary, N., . . . Szerlip, N. J. (2017). An integrated multidisciplinary algorithm for the management of spinal metastases: an International Spine Oncology Consortium report. *Lancet Oncol, 18*(12), e720-e730. doi:10.1016/S1470-2045(17)30612-5

Suri, S. S., Fenniri, H., & Singh, B. (2007). Nanotechnology-based drug delivery systems. *J Occup Med Toxicol, 2*, 16. doi:10.1186/1745-6673-2-16

Teixeira, S., Branco, L., Fernandes, M. H., & Costa-Rodrigues, J. (2019). Bisphosphonates and Cancer: A Relationship Beyond the Antiresorptive Effects. *Mini Rev Med Chem, 19*(12), 988-998. doi:10.2174/1389557519666190424163044

Umunakwe, O. C., Herren, D., Kim, S. J., & Kohanim, S. (2017). Diffuse ocular and orbital inflammation after zoledronate infusion-case report and review of the literature. *Digit J Ophthalmol, 23*(4), 18-21. doi:10.5693/djo.02.2017.08.002

Wai, E. K., Finkelstein, J. A., Tangente, R. P., Holden, L., Chow, E., Ford, M., & Yee, A. (2003). Quality of life in surgical treatment of metastatic spine disease. *Spine (Phila Pa 1976), 28*(5), 508-512. doi:10.1097/01.BRS.0000048646.26222.FA

Walker, M. P., Yaszemski, M. J., Kim, C. W., Talac, R., & Currier, B. L. (2003). Metastatic disease of the spine: evaluation and treatment. *Clin Orthop Relat Res*(415 Suppl), S165-175. doi:10.1097/01.blo.0000092977.12414.f9

Walsh, G. L., Gokaslan, Z. L., McCutcheon, I. E., Mineo, M. T., Yasko, A. W., Swisher, S. G., . . . Roth, J. A. (1997). Anterior approaches to the thoracic spine in patients with cancer: indications and results. *Ann Thorac Surg, 64*(6), 1611-1618. doi:10.1016/s0003-4975(97)01034-5

Wang, Z., Kumar, H., Tian, Z., Jin, X., Holzman, J. F., Menard, F., & Kim, K. (2018). Visible Light Photoinitiation of Cell-Adhesive Gelatin Methacryloyl Hydrogels for Stereolithography 3D Bioprinting. *ACS Appl Mater Interfaces, 10*(32), 26859-26869. doi:10.1021/acsami.8b06607

Wei, L., Hu, N., & Zhang, Y. (2010). Synthesis of Polymer-Mesoporous Silica Nanocomposites. *Materials (Basel), 3*(7), 4066-4079. doi:10.3390/ma3074066

Widler, L., Jahnke, W., & Green, J. R. (2012). The chemistry of bisphosphonates: from antiscaling agents to clinical therapeutics. *Anticancer Agents Med Chem, 12*(2), 95-101. doi:10.2174/187152012799014959

Wilczewska, A. Z., Niemirowicz, K., Markiewicz, K. H., & Car, H. (2012). Nanoparticles as drug delivery systems. *Pharmacol Rep, 64*(5), 1020-1037. doi:10.1016/s1734-1140(12)70901-5

Yang, J., Guo, Y., Lu, C., Zhang, R., Wang, Y., Luo, L., . . . Li, X. (2019). Inhibition of Karyopherin beta 1 suppresses prostate cancer growth. *Oncogene, 38*(24), 4700-4714. doi:10.1038/s41388-019-0745-2

Yasuda, H., Shima, N., Nakagawa, N., Yamaguchi, K., Kinosaki, M., Mochizuki, S., . . . Suda, T. (1998). Osteoclast differentiation factor is a ligand for osteoprotegerin/osteoclastogenesis-inhibitory factor and is identical to TRANCE/RANKL. *Proc Natl Acad Sci U S A, 95*(7), 3597-3602. doi:10.1073/pnas.95.7.3597

Zhang, Y. S., Arneri, A., Bersini, S., Shin, S. R., Zhu, K., Goli-Malekabadi, Z., . . . Khademhosseini, A. (2016). Bioprinting 3D microfibrous scaffolds for engineering endothelialized myocardium and heart-on-a-chip. *Biomaterials, 110*, 45-59. doi:10.1016/j.biomaterials.2016.09.003

Zhou, X., Zhu, W., Nowicki, M., Miao, S., Cui, H., Holmes, B., . . . Zhang, L. G. (2016). 3D Bioprinting a Cell-Laden Bone Matrix for Breast Cancer Metastasis Study. *ACS Appl Mater Interfaces, 8*(44), 30017-30026. doi:10.1021/acsami.6b10673